Universiteit
Leiden
The Netherlands

Role of metabolic pathways and sensors in regulation of dendritic cell-driven T cell responses

Pelgrom, L.R.

Citation

Pelgrom, L. R. (2022, February 23). *Role of metabolic pathways and sensors in regulation of dendritic cell-driven T cell responses*. Retrieved from https://hdl.handle.net/1887/3275848

Version:	Publisher's Version
License:	Licence agreement concerning inclusion of doctoral thesis in the Institutional Repository of the University of Leiden
Downloaded from:	https://hdl.handle.net/1887/3275848

Note: To cite this publication please use the final published version (if applicable).

9

mTORC1 signalling in antigen-presenting cells of the skin restrains CD8+ T cell priming

Leonard R. Pelgrom
Thiago A. Patente
Frank Otto
Lonneke V. Nouwen
Arifa Ozir-Fazalalikhan
Alwin J. van der Ham
Hendrik J.P. van der Zande
Ramon Arens
Bart Everts

Under revision

Abstract

Mechanistic target of rapamycin complex 1 (mTORC1), a key sensor and regulator of cellular metabolism, has primarily been shown *in vitro* to affect various aspects of dendritic cell (DC) biology. However, our understanding of how mTORC1 regulates DC metabolism and their T cell-priming capacity *in vivo* remains limited. Here, using mice deficient in mTORC1 component raptor in DCs ($CD11c^{\Delta raptor}$), we found that loss of mTORC1 primarily compromises glucose uptake, mitochondrial fitness and cellular maturation, particularly MHCI expression, of type 1 conventional DCs from lymphoid organs. Nonetheless, antigen-specific CD8+ T cell responses to infection were not compromised and even enhanced following skin immunization in $CD11c^{\Delta raptor}$ mice. This was associated with potentiated costimulatory molecule expression and IL-12 production specifically by Langerhans cells in $CD11c^{\Delta raptor}$ mice. Together, this work reveals distinct roles for mTORC1 in orchestrating the immunogenicity of different antigen presenting cell subsets, which may have implications for vaccination practices.

Introduction

Dendritic cells (DCs) of the innate immune system are uniquely equipped to present antigens to T cells and to provide costimulatory signals and cytokines for T cell activation and polarization. This gives them a central role in the establishment of protective adaptive immunity following infections and after vaccination. In addition, their ability to prime regulatory T cells and their ability to induce anergy to host self-antigens, make them critical regulators of tolerance [1]. DCs patrol tissues until they recognize exogenous or endogenous danger signals with their pattern recognition receptors, after which they undergo rapid changes in their biology that enable them to efficiently migrate to lymphoid tissues and instruct T cells there for the appropriate immune response [2]. As these changes require concomitant changes in their metabolism [3], manipulation of DC metabolism may become an attractive therapeutic strategy for controlling the outcome of immune responses.

The mechanistic (formerly mammalian) target of rapamycin (mTOR) coordinates intracellular metabolism with environmental inputs that include nutrients, growth factors and immunological cues such as cytokines. It is a protein complex that exists in two distinct forms with either raptor (mTOR complex 1 [mTORC1]) or rictor (mTORC2) as one if its core components. Activity of mTORC1 is associated with increased protein synthesis, metabolism of lipids, nucleotides and glucose, and reduced autophagy; while mTORC2 signalling governs proliferation, survival, and cytoskeletal remodelling. Of the two, mTORC1 has been investigated most thoroughly, due to the discovery in the early 1970s of the compound 'rapamycin', which gave the complex it inhibited its name [4]. mTORC1 signalling has been shown to be vital for the metabolic reprogramming of various immune cells and in particular for the initial activation, proliferation, differentiation and effector function acquisition of lymphocytes [5].

The role of mTORC1 in DC biology has been extensively studied *in vitro*, and the outcome of mTORC1 inhibition in these cells seems to be context and species dependent [6, 7]. In vivo transferred murine bone marrow-derived DCs (BMDCs), that were generated *in vitro* using granulocyte-macrophage colony-stimulating factor (GM-CSF [GMDCs]), were shown to prime stronger CD8+ T cell responses after toll-like receptor (TLR)-activated in the presence of rapamycin [8-10]. This was associated with increased autophagy [10], a switch from anaerobic glycolysis to oxidative phosphorylation [11], and increased longevity and maintenance of high costimulatory molecule expression [8]. These latter two effects are likely the result of autocrine signalling by nitric oxide (NO) [12, 13], so whether these findings translate to conventional DCs (cDCs) that express little NO *in vivo* [14] is currently unclear.

Thus far, *in vivo* studies using CD11c-cre raptor$^{fl/fl}$ mice that display a selective loss of mTORC1 signalling in CD11c-expressing cells, which is largely restricted to DCs, revealed that maintenance of CD103+ type 1 cDCs (cDC1s) in the lungs [15] and Langerhans cells (LCs) in the skin and to a lesser degree in draining lymph nodes [16], was dependent on mTORC1 signalling. In addition, frequencies of CD8+ cDC1s in the spleen and CD11b+ cDC2s in the lamina propria can be modulated by loss of mTORC1 signalling [17], although the changes in DC homeostasis were not nearly as affected as in the lungs [15]. Functionally, mice with a CD11c-specific mTOR deletion, in which both mTORC1 and mTORC2 signalling is compromised, were found to have an antigen presenting cell (APC) compartment in the lung with an altered cellular metabolism, which was associated with a reduced capacity to mount a CD8+ T cell response upon viral infection and directly responsible for a shift from mounting a type 2 to type 17 immune response following allergen challenge [15]. However, whether these effects are a consequence of a defect in mTORC1, mTORC2 signalling, or both, remains unclear. Hence the specific role of mTORC1 signalling in DCs in regulating their metabolic and T cell-priming phenotype *in vivo* remains to be addressed.

In the current study, we found that the loss of raptor, a key component of mTORC1, in DCs compromises the maturation of various DC subsets in the spleen and skin draining lymph nodes, which was apparent during steady state conditions, systemic infection and local immunization. Especially the surface expression of the major histocompatibility complex I (MHCI) was reduced, which was associated with selective metabolic defects in cDC1s. Nevertheless, the priming of CD8+ T cells was not impaired but rather potentiated following subcutaneous (s.c.) immunization. This latter finding was associated specifically with enhanced IL-12 production and costimulatory molecule surface expression by LCs. Together, these data provide new insights into APC subset-specific effects of mTORC1 signalling and how this controls T cell responses *in vivo*, with a potential role for mTORC1 in restricting LC-dependent CD8+ T cell priming.

Results

mTORC1 signalling impacts glucose uptake and MHCI expression by splenic cDC1s

Mice with a conditional deletion of raptor in CD11c-expressing cells ($CD11c^{\Delta raptor}$ mice) displayed decreased steady state phosphorylation of ribosomal protein S6, a downstream target of the mammalian target of rapamycin complex 1 (mTORC1) that contains raptor, in both type 1 (cDC1) and type 2 splenic conventional DCs (cDC2) (Figure 1B). In contrast to what was previously reported [17], the frequency and numbers of splenic cDC1s were similar between CD11c-cre negative $raptor^{fl/fl}$ ($CD11c^{WT}$) and $CD11c^{\Delta raptor}$ littermates (Figure 1A,C). However, we did observe changes in splenic cDC1 metabolism. In keeping with reports that splenic cDC1s are more metabolically active than splenic cDC2s [18], we found splenic cDC1s to have higher uptake of the fluorescent glucose analogue 2-NBDG than other splenic DC subsets (Figure 1D). And consistent with a well described role for mTORC1 signalling in supporting glycolysis [4-7], we found that conditional deletion of raptor lowered 2-NBDG uptake in cDC1s, but not in cDC2s and pDCs (Figure 1D). Loss of raptor did not affect mitochondrial mass and membrane potential of any DC subset in the spleen (Figure 1E). Given the importance of glycolysis in DC activation [19-21], we next investigated whether the selective reduction of 2-NBDG uptake in raptor-deficient cDC1s was accompanied by changes in surfaces markers related to DC activation. Conditional deletion of raptor in splenic cDCs primarily resulted in an impaired activation profile of splenic cDC1s of which a decrease in MHCI surface expression was most prominent (Figure 1F).

Figure legends

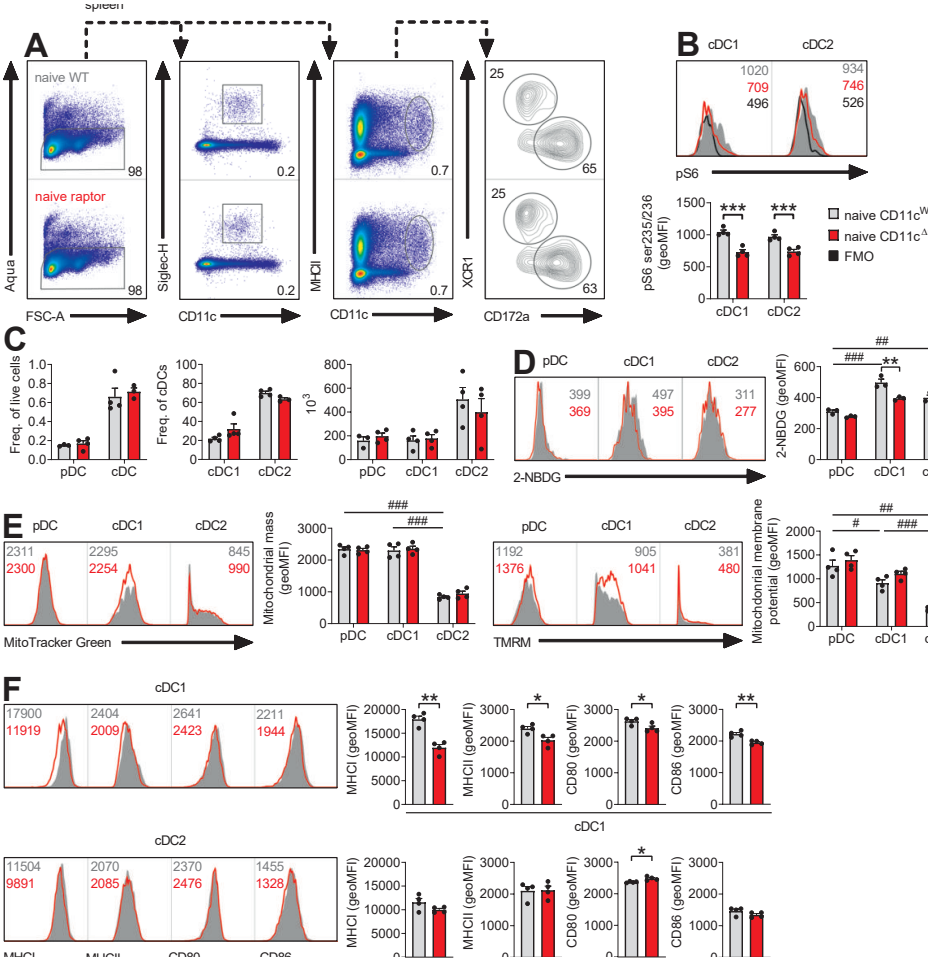

CD8+ T cell priming in response to, and host protection against listeria infection is intact in mice with raptor-deficient APCs

Given the critical role for MHCI in the priming and maintenance of CD8+ T cells by DCs, we next assessed whether the reduced expression of MHCI on raptor-deficient splenic cDCs would affect the CD8+ T cell pool in CD11c$^{\Delta raptor}$ mice. Indeed, in naïve CD11c$^{\Delta raptor}$ mice, antigen-experienced effector (EFF; CD44+CD62L-) CD8+ T cells were reduced in blood and central memory (CM; CD44+CD62L+) CD8+ T cells were reduced spleen, despite normal T cell development in the thymus (Figure 2A and S1A-B).

Figure 1. mTORC1 signalling is required for glucose uptake by splenic cDC1s and their MHCI expression.

(A) Flow gating strategy for splenic DC subsets by sequential gating of intact cells (forward scatter area [FSC-A] versus side scatter area [SSC-A], not shown), singlets (FSC-A versus forward scatter height [FSC-H], not shown), live cells (Aqua- cells in panel 1), pDCs (CD11c+ versus Siglec-H+ cells in panel 2) and cDCs (CD11c++ versus MHCII+ cells in panel 3), cDC1s (XCR1+ or CD8+ versus CD172a- or CD11b- cells in panel 4) and cDC2s (XCR1- or CD8- versus CD172a+ or CD11b+ cells in panel 4). (B) Flow cytometry-based analysis of S6 phosphorylation on serine 235/236 in splenic cDCs from $CD11c^{WT}$ mice in grey, $CD11c^{\Delta raptor}$ mice in red and a Fluorescence Minus One (FMO) control in black. (C) Frequencies and numbers of splenic DC subsets as gated in A) are enumerated. (D) Flow cytometry-based analysis of overall metabolic pathway engagement by splenic DC subsets using the fluorescent glucose analogue 2-NBDG. (E) Flow cytometry-based analysis of mitochondrial mass and mitochondrial membrane potential in splenic DC subsets using MitoTracker Green and TMRM respectively. (F) Flow cytometry-based analysis of MHCI, MHCII, CD80 and CD86 surface protein expression on splenic cDCs. Data are from 1 out of 2 representative experiments using 3-4 mice per group and shown as mean ± SEM; $*p < 0.05$, $**p < 0.01$, $***p < 0.001$ when comparing samples between $CD11c^{WT}$ and $CD11c^{\Delta raptor}$ mice; $\#\#p < 0.01$, $\#\#\#p < 0.001$ when comparing populations within $CD11c^{WT}$ mice.

Next, to determine whether CD8+ T cell responses in $CD11c^{\Delta raptor}$ mice would be similarly compromised in response to infection, mice were challenged with a live-attenuated strain of *Listeria monocytogenes* expressing ovalbumin (Lm-dActA-OVA). *L. monocytogenes* is a facultative intracellular bacterium that primarily infects the spleen and liver and largely depends on splenic cDC1s for the efficient priming of protective CD8+ T cell responses [22]. While the infection elicited a clear expansion of CD44+CD62L- effector CD8+ T cells in control mice, this was less pronounced in the spleens of $CD11c^{\Delta raptor}$ mice after infection (Figure 2B-C). However, within this effector pool, the frequency of OVA-specific CD8+ T cells was increased in these mice. This resulted in a similar overall number of OVA-specific CD8+ T cells in the spleens of infected WT and $CD11c^{\Delta raptor}$ mice (Figure 2D). The expansion of CD44+ effector CD4+ T cells was affected to a lesser degree (Figure 2C) and their capacity to produce cytokines was unaltered (Figure S1C). In contrast, the production of the prototypical CD8+ cytotoxic T cell (CTL) cytokine interferon-gamma (IFNγ) by CD44+ CD8+ T cells in spleens from $CD11c^{\Delta raptor}$ mice after *ex vivo* restimulation with OVA was higher than that of CD8+ T cells from $CD11c^{WT}$ mice (Figure 2E). Together, this suggests that the ability of $CD11c^{\Delta raptor}$ mice to mount antigen-specific CD8+ T cell responses to Lm-dActA-OVA infection was not compromised.

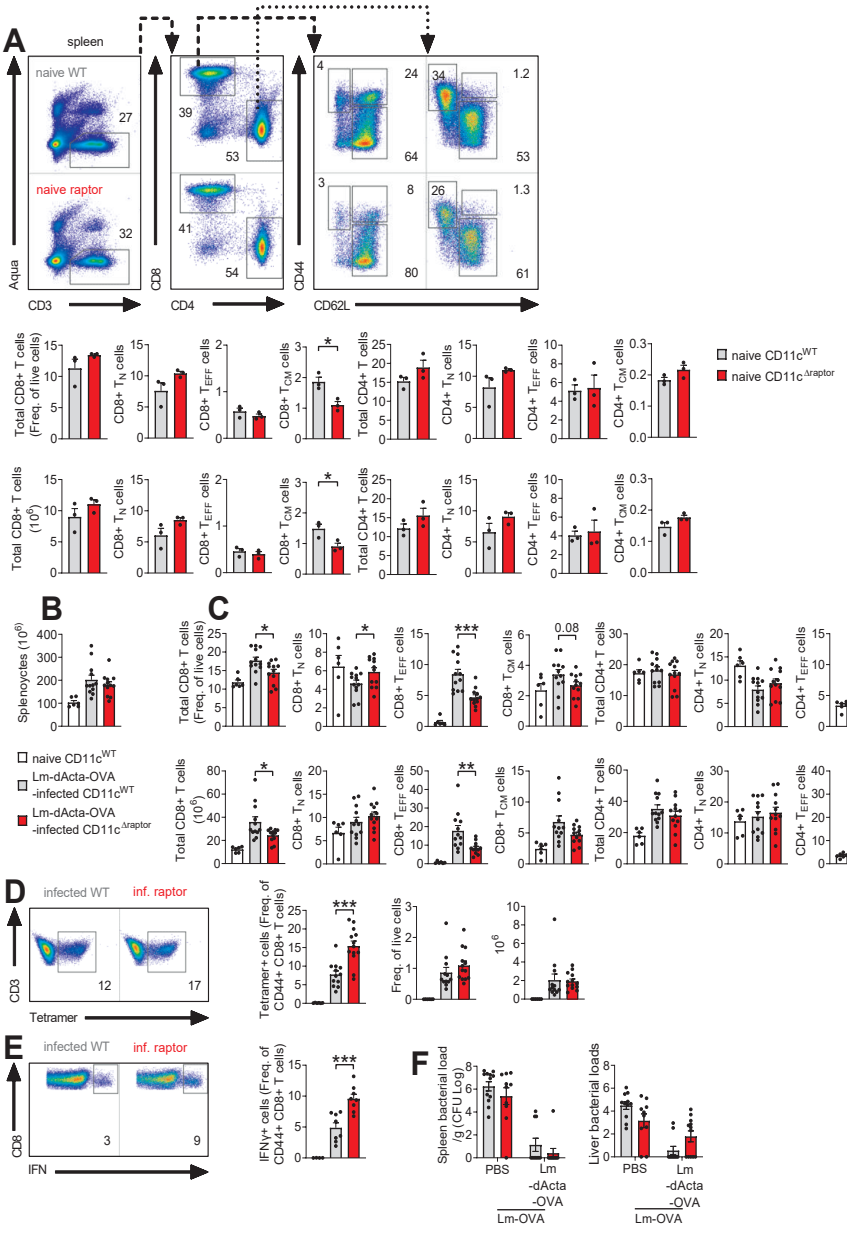
A
spleen
naive WT
naive raptor
Aqua
CD3
CD8
CD4
CD44
CD62L
naive CD11c^WT
naive CD11c^Δraptor
B
C
Splenocytes (10^6)
Lm-dActa-OVA -infected CD11c^WT
Lm-dActa-OVA -infected CD11c^Δraptor
D
infected WT
inf. raptor
Tetramer
E
IFN
F
Spleen bacterial load /g (CFU Log)
Liver bacterial loads
PBS
Lm -dActa -OVA
Lm-OVA

Figure 2. CD8+ T cell priming in response to Listeria infection and host protection is intact in mice with raptor-deficient APCs.

(A) On the top a gating strategy for splenic T cell subsets by sequential gating of intact cells (forward scatter area [FSC-A] versus side scatter area [SSC-A], not shown), singlets (FSC-A versus forward scatter height [FSC-H], not shown), live cells (Aqua- cells in panel 1), live T cells (CD3+ versus Aqua- cells in panel 1), total CD4 T cells (CD4+ versus CD8+ in panel 2) and total CD8+ T cells (CD4- versus CD8+ in panel 2), naïve CD8+ T cells (CD8+ TN; CD62L+ versus CD44- in panel 3) and effector CD8+ T cells (CD8+ TEFF; CD62L- versus CD44+ in panel 3) and central memory CD8+ T cells (CD8+ TCM; CD62L+CD44+ in panel 3), and naïve CD4 T cells (CD4+ TN; CD62L+CD44- in panel 4) and effector CD4 T cells (CD4+ TEFF; CD62L- versus CD44+ in panel 4) and central memory CD4+ T cells (CD4+ TCM; CD62L+CD44+ in panel 4). Antigen-experienced T cells (TAE) are the sum of TEFF and TCM subsets. Frequencies and numbers of splenic T cells are enumerated on the bottom. (B-E) $CD11c^{WT}$ and $CD11c^{\Delta raptor}$ mice were infected with 5x10^6 Lm-dActa-OVA i.v. and splenic T cell responses were analysed 7 days later by flow cytometry. (B) Total cell numbers in spleen. (C) Frequencies and numbers of splenic CD8+ T cell subsets as analysed by flow cytometry. Representative histograms are in Figure S1A. (D) Frequencies and numbers of OVA-specific CD8+ TAE cells based on K^bOVA-tetramer staining as analysed by flow cytometry. (E) Splenocytes were stimulated with SIINFEKL in the presence of Brefeldin A and analysed for OVA-specific IFNγ production by CD8+ TAE cells using flow cytometry. (F) Mice were infected with 5x106 Lm-dActa-OVA by retro-orbital i.v. injection and challenged 21 days later with 5x104 Lm-OVA. The burden of LM-OVA in spleen and liver were determined on day 24. Data are from 2 experiments using 1-3 mice per group (A), 3 experiments using 1-4 mice per group (B-E, although E misses 1 experiment due to failed T cell marker staining), or 2 experiments using 5-7 mice per group (F). Data shown as mean ± SEM; $*p < 0.05$, $***p < 0.001$ when comparing samples between $CD11c^{WT}$ and $CD11c^{\Delta raptor}$ mice.

To assess whether the differences between the CD8+ T cell compartments of $CD11c^{WT}$ and $CD11c^{\Delta raptor}$ mice following a primary infection with attenuated Lm-dActA-OVA would affect protective immunity against a secondary infection with a replication competent strain (Lm-OVA), mice were infected as before and subsequently challenged with Lm-OVA three weeks later. Right before challenge (d20 post primary infection) no differences in frequencies of circulating CM or effector OVA-specific CD8+ T cells between $CD11c^{WT}$ and $CD11c^{\Delta raptor}$ mice were observed (Figure S1D). Moreover, 3 days following challenge infection (d24 post primary infection) frequencies of effector, antigen-experienced (AE; CD44+) CD8+ T cells in blood and spleen were comparable between $CD11c^{WT}$ and $CD11c^{\Delta raptor}$ mice (Figure S1D). In line with these results, the bacterial loads in spleen and liver did not significantly differ between the two groups (Figure 2F), suggesting that CD8+ T cell memory formation and protective immunity to *L. monocytogenes* rechallenge was not affected by the loss of raptor in CD11c-expressing cells.

mTORC1 signalling is dispensable for longevity, maturation duration and production of IL-12 and IL-10 by TLR-stimulated splenic DCs

To mechanistically understand how CD11c$^{\Delta raptor}$ mice generated increased frequencies of antigen-specific and IFNγ-producing CD8+ T cells in response to *L. monocytogenes* infection, despite having splenic cDC1s with decreased surface expression of MHCI, we first assessed whether infection restored or even further enhanced levels of MHCI on these DCs. However, raptor-deficient splenic cDC1s maintained a decreased surface expression of MHCI following infection with Lm-dActA-OVA (Figure 3A). Since cross-presentation by DCs has been demonstrated to contribute to proper priming of CD8+ T cell responses against *L. monocytogenes* infection [23] and that autophagy, a process known to be enhanced by mTORC1 inhibition [4], can promote cross-presentation [24], we tested whether this was enhanced in DCs lacking raptor. However, the capacity of raptor-deficient cDC1s to cross-present soluble antigen - as assessed by their ability to present the H-2Kb-restricted $OVA_{257-264}$ short peptide (SIINFEKL) on MHCI following exposure to a synthetic long peptide (SLP) variant that contains this epitope (SLP-OVA) - was lower than that of their CD11c^{WT} counterparts (Figure 3B).

As rapamycin can promote GMDC longevity and sustain high costimulatory molecules expression after TLR stimulation [8], we next assessed survival and/or maturation comparing splenic cDCs from CD11c^{WT} and CD11c$^{\Delta raptor}$ mice following *ex vivo* TLR stimulation of whole splenocyte cultures for several days. However, no differences in survival (Figure S2A) or maturation (Figure S2B) were observed. As it has been shown that also IL-12 production by cDC1s can play a key role in the production of IFNγ by CD8+ T cells [25] and - primarily based on mouse GMDCs culture and human primary DC data - it is known that mTORC1 signalling can limit the production of IL-12 by DCs [6], we additionally tested whether there was a difference in IL-12p40/p70 production between splenic cDCs from CD11c^{WT} and CD11c$^{\Delta raptor}$ mice. However, IL-12 production by splenic cDCs from naïve CD11c$^{\Delta raptor}$ and CD11c$^{\Delta raptor}$ mice that were stimulated *ex vivo* with TLR ligands was comparable (Figure 3C). Alternatively, rapamycin-sensitive IL-10 production by DCs can limit CD8+ T cell priming independent of IL-12 production [26] and because conditional deletion of raptor in CD11c-expressing cells has been shown to abolish the steady state production of IL-10 by DCs and macrophages from the small intestine [17], we went on to determine whether there was a difference in IL-10 secretion between sorted splenic cDC1s and cDC2s from CD11c^{WT} and CD11c$^{\Delta raptor}$ mice, in which the DC numbers were expanded *in vivo* using Flt3L. However, the IL-10 production after *ex vivo* stimulation with the TLR3 ligand PolyIC was not significantly different (Figure 3D). More importantly, when we immunized recipient mice with these

cDC1s, no differences were observed in their CD8+ T cell priming capacity (Figure 3E-H).

Taken together, these data suggest that raptor deficiency in cDC1s compromises MHCI expression and cross presentation, without significantly affecting longevity, maturation duration, cytokine production and CD8+ T cell priming.

mTORC1 signalling is required for maintenance of mitochondrial mass in skin migratory cDC1s and supports maturation of both migratory cDC subsets

mTOR signalling impacts DC biology differently depending on the tissue the DCs reside in [15], which made us wonder if DCs in other lymphoid tissues than the spleen, such as skin draining lymph nodes (sdLNs), would be similarly affected by loss of raptor with respect to their metabolic and immunogenic phenotype. Phosphorylation of ribosomal protein S6 showed a trend to be decreased in raptor-deficient cDCs from sdLNs (Figure 4B and S3A), suggesting a functional loss of raptor also in these DCs. This loss might potentiate their migration under steady state conditions as both the frequency and number of migratory cDCs (migDCs) were higher in sdLNs from $CD11c^{\Delta raptor}$ mice compared to $CD11c^{WT}$ mice (Figure 4A,C). In contrast, resident DC (resDC) homeostasis was unchanged (Figure 4A,C). Like splenic cDC1s, skin migDC1s showed high 2-NBDG uptake, high mitochondrial mass and high membrane potential, of which the former was reduced by loss of raptor (Figure 4D-E and S3B). Moreover, like in the spleen, raptor deficiency more severely blunted maturation of sdLN migDC1 than that of sdLN migDC2s, as evaluated by the decreased surface expression of MHCI, MHCII, CD86 and CD80 on migDC1s versus MHCI and MHCII on migDC2s (Figure 4F and S3C). Together, these data reveal that also in skin-draining LNs the phenotype of cDC1s is more severely impacted by loss of raptor than that of cDC2s.

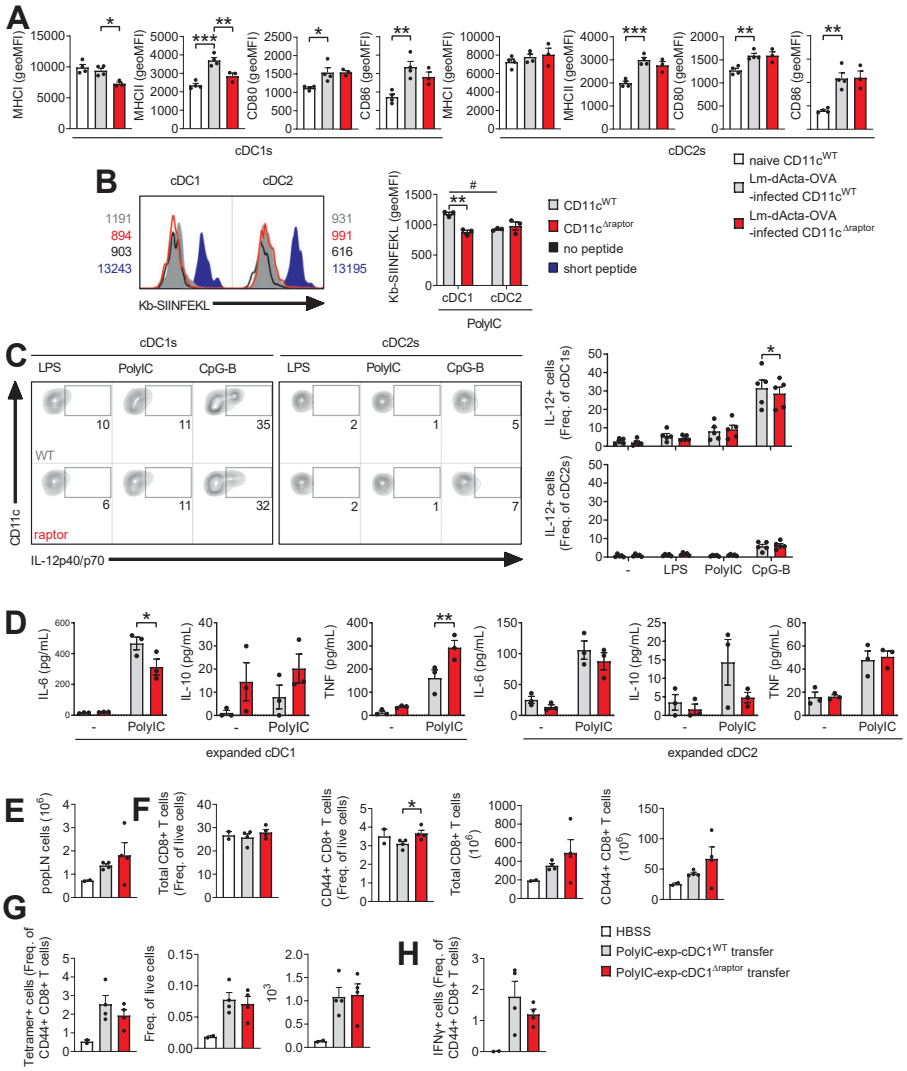
A
MHCI (geoMFI)
MHCII (geoMFI)
CD80 (geoMFI)
CD86 (geoMFI)
cDC1s
cDC2s
B
cDC1
cDC2
Kb-SIINFEKL
naive CD11c^WT
Lm-dActa-OVA -infected CD11c^WT
Lm-dActa-OVA -infected CD11c^Δraptor
CD11c^WT
CD11c^Δraptor
no peptide
short peptide
PolyIC
C
cDC1s
cDC2s
LPS
PolyIC
CpG-B
WT
raptor
CD11c
IL-12p40/p70
IL-12+ cells (Freq. of cDC1s)
IL-12+ cells (Freq. of cDC2s)
D
IL-6 (pg/mL)
IL-10 (pg/mL)
TNF (pg/mL)
expanded cDC1
expanded cDC2
E
popLN cells (10^6)
F
Total CD8+ T cells (Freq. of live cells)
CD44+ CD8+ T cells (Freq. of live cells)
Total CD8+ T cells (10^6)
CD44+ CD8+ T cells (10^6)
G
Tetramer+ cells (Freq. of CD44+ CD8+ T cells)
Freq. of live cells
H
IFNγ+ cells (Freq. of CD44+ CD8+ T cells)
HBSS
PolyIC-exp-cDC1^WT transfer
PolyIC-exp-cDC1^Δraptor transfer

Figure 3. mTORC1 signalling is dispensable for longevity, maturation duration and production of IL-12 and IL-10 by TLR-stimulated splenic DCs.

(A) $CD11c^{WT}$ and $CD11c^{\Delta raptor}$ mice were infected with 2.5x10^5 Lm-dActA-OVA by retro-orbital i.v. injection and splenic cDCs surface protein expression of indicated surface markers was analysed 1 day later by flow cytometry. (B) Flow cytometry-based analysis of cross presentation in splenic cDCs from $CD11c^{WT}$ mice in grey, $CD11c^{\Delta raptor}$ mice, a no antigen negative control in black and a SIINFEKL positive control in blue. (C) Splenocytes from naïve WT and $CD11c^{\Delta raptor}$ mice were stimulated with either 100 ng/mL LPS, 10 µg/mL PolyIC or 5 µg/mL CpG-B and all in the presence of Brefeldin A and analysed for production of IL-12p40/p70 by splenic cDCs using flow cytometry. (D) In vivo Flt3L-expanded splenic cDC1s and cDC2s were sorted using a flow cytometer and put into culture with or without PolyIC. Supernatants were harvested 16 hours later and analysed for indicated cytokines by cytokine bead array. (E-H) In vivo Flt3L-expanded splenic cDC1s were sorted and conditioned with OVA and PolyIC for 5 hours *ex vivo* before transfer into recipient mice by footpad injection. CD8+ T cell responses were evaluated in draining popliteal LNs (popLNs) 7 days later by flow cytometry. (E) Number of cells in popLNs. (F) Frequencies and numbers of total CD8+ T cells and antigen-experienced (CD44+) CD8+ T cells (CD8+ TAE) as analysed by flow cytometry. (G) Frequencies and numbers of OVA-specific CD8+ TAE cells based on K^bOVA-tetramer staining as analysed by flow cytometry. (H) Splenocytes were stimulated with SIINFEKL in the presence of Brefeldin A and analysed for OVA-specific IFNγ production by CD8+ TAE cells using flow cytometry. Data are from 1 experiment using 4 mice per group (A), 1 experiment using 3 mice per group (B) 5 experiments using 1 mouse per group (C), 1 experiment using 3 mice per group (D), or 1 experiment using 2-4 mice per group (E-H). Data shown as mean ± SEM; $*p < 0.05$, $**p < 0.01$, $***p < 0.001$ when comparing samples between $CD11c^{WT}$ and $CD11c^{\Delta raptor}$ mice; $\#p < 0.05$ when comparing populations within $CD11c^{WT}$ mice.

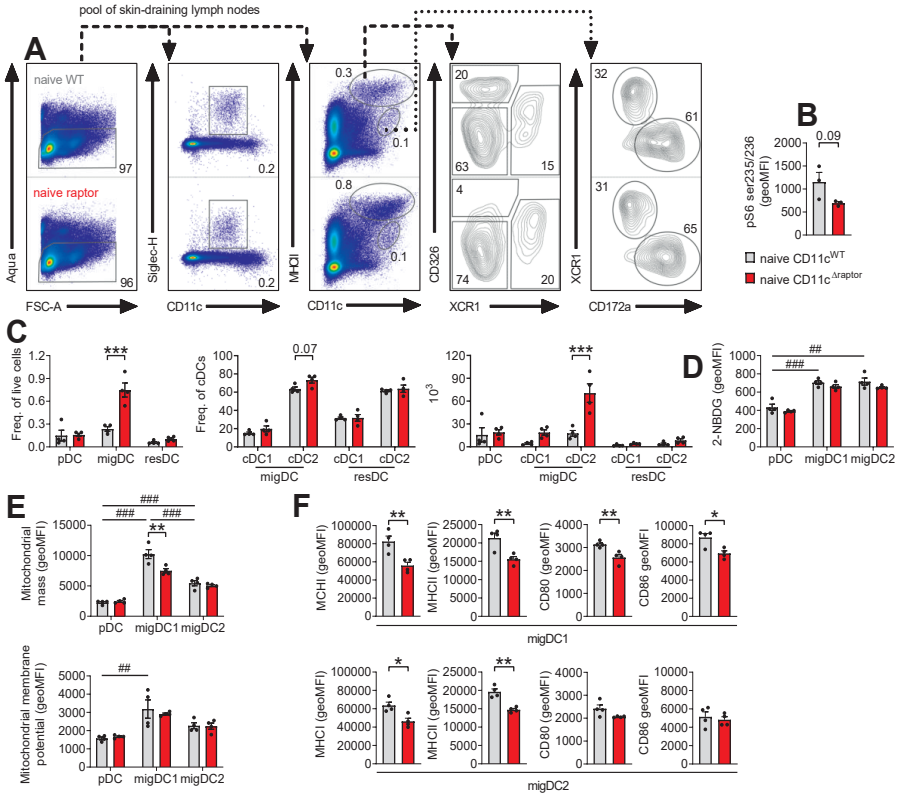
pool of skin-draining lymph nodes
A
naive WT
naive raptor
Aqua
FSC-A
SiglecH
CD11c
MHCII
CD11c
CD326
XCR1
XCR1
CD172a
B
pS6 ser235/236 (geoMFI)
naive CD11c^WT
naive CD11c^Δraptor
C
Freq. of live cells
Freq. of cDCs
10^3
pDC
migDC
resDC
cDC1
cDC2
D
2-NBDG (geoMFI)
pDC
migDC1
migDC2
E
Mitochondrial mass (geoMFI)
Mitochondrial membrane potential (geoMFI)
F
MCHI (geoMFI)
MHCII (geoMFI)
CD80 (geoMFI)
CD86 geoMFI
migDC1
migDC2

Figure 4. mTORC1 signalling is required for maintenance of mitochondrial mass in skin migratory cDC1s and supports maturation of both migratory cDC subsets.

(A) Flow gating strategy for LCs and DC subsets in sdLNs by sequential gating of intact cells (forward scatter area [FSC-A] versus side scatter area [SSC-A], not shown), singlets (FSC-A versus forward scatter height [FSC-H], not shown), live cells (Aqua- cells in panel 1), pDCs (CD11c+ versus Siglec-H+ cells in panel 2) and migratory APCs (CD11c+ versus MHCII++ cells in panel 3) and resDCs (CD11c+ versus MHCI+ cells in panel 3), LCs (XCR1- versus CD326+ cells in panel 4) and migDC1s (XCR1+ versus CD326- in panel 4) and migDC2s (XCR1- versus CD326- in panel 4), and resDC1s (CD172a- versus XCR1+ cells in panel 5) and resDC2s (CD172a+ versus XCR1- cells in panel 5). (B) Flow cytometry-based analysis of S6 phosphorylation on serine 235/236 in total migDCs from skin draining lymph nodes (sdLNs) out of $CD11c^{WT}$ mice in grey, $CD11c^{\Delta raptor}$ mice in red and a Fluorescence Minus One (FMO control in black). Representative histograms are in Figure S3A. sdLNs were a pool of brachial, axillary and inguinal LNs. (C) Frequencies and numbers of DC subsets in sdLNs as gated in A) are enumerated. Migratory DCs are migAPCs minus LCs. (D) Flow cytometry-based analysis of overall metabolic pathway engagement by sdLN DC subsets using the fluorescent glucose analogue 2-NBDG. Representative histograms are in Figure S3B. (E) Flow cytometry-based analysis of mitochondrial mass and mitochondrial membrane potential in sdLN DC subsets using MitoTracker Green and TMRM respectively. Representative histograms are in Figure S3B. (F) Flow cytometry-based analysis of MHCI, MHCII, CD80 and CD86 surface protein expression on sdLN migDCs. Representative histograms are in Figure S6C. Data are from 1 out of 2 representative experiments using 4 mice per group and shown as mean ± SEM; *p < 0.05, **p < 0.01, ***p < 0.001 when comparing samples between WT and $CD11c^{\Delta raptor}$ mice; ##p < 0.01, ###p < 0.001 when comparing populations within $CD11c^{WT}$ mice.

mTORC1 signalling in CD11c-expressing cells limits CD8+ T cell priming following subcutaneous immunization

Because raptor-deficient sdLN migDC1s and migDC2s displayed a weaker maturation profile, we first investigated if the T cell compartment in sdLNs from $CD11c^{\Delta raptor}$ mice was changed under steady state conditions. Like in the circulation, the frequency of effector T cells was reduced in sdLNs from naïve $CD11c^{\Delta raptor}$ mice compared to $CD11c^{WT}$ mice (Figure 5A).

sdLN migDC2s from $CD11c^{\Delta raptor}$ mice express reduced MHCII (Figure 4F), which has been implicated in favouring the priming of CD4+ T helper 2 (Th2) cells [27]. In addition, pharmacological inhibition of mTORC1 in human monocyte-derived DCs has been shown to enhance their Th2-priming capacity *in vitro* [28]. Hence, we next investigated whether Th2 priming was altered in $CD11c^{\Delta raptor}$ mice following footpad injection with a soluble antigen extract of *Schistosoma mansoni* eggs (SEA). However, the secretion of canonical type 2 cytokines such as IL-4, IL-5, and IL-13 by sdLN cells from $CD11c^{WT}$ and $CD11c^{\Delta raptor}$ mice was comparable after *ex vivo* antigen-specific restimulation (Figure 5B). Moreover, Th2 responses were not different between $CD11c^{WT}$ and $CD11c^{\Delta raptor}$

mice during systemic *S. mansoni* infection, as evaluated by the production of type 2 cytokines by CD44+CD4+ cells in the liver and draining hepatic lymph node (Figure S4), which are major sites of T cell priming during schistosomiasis [29]. Together, these data suggest that mTORC1 signalling in CD11c-expressing cells is not important for the generation of Th2 cell responses.

Finally, we assessed whether the reduced activation profile of sdLN migDC1s in CD11c$^{\Delta raptor}$ mice would affect CD8+ T cell priming following s.c. immunization. Mice were immunized with the TLR9 ligand CpG-B in combination with a synthetic 43-mer long peptide form the human papillomavirus (HPV) E7 protein that contains the immunodominant and H-2Db-restricted epitope RAHYNIVTF (E7-SLP), a combination that predominantly activates cDC1s and requires cross-presentation for priming of CD8+ T cells [30]. This resulted in enhanced frequencies and numbers of E7-specific CD8+ T cells in sdLNs from CD11c$^{\Delta raptor}$ mice compared to sdLNs from their CD11c^{WT} littermates (Figure 5C-D), as well as enhanced IFNγ production by these cells after *ex vivo* antigen-specific restimulation (Figure 5E-F). These effects were independent of antigen or TLR stimulus, as enhanced IFNγ production by CD8+ T cells and trends towards higher frequencies and numbers of antigen-specific CD8+ T cells were also observed in CD11c$^{\Delta raptor}$ mice after immunization with CpG-B with full length OVA (Figure 5G-J) or PolyIC with E7-SLP (Figure 5K-L).

mTORC1 signalling supports activation of migratory skin DCs but constrains activation of Langerhans cells in response to subcutaneous immunization

To find a mechanistic basis for the enhanced IFNγ production by CD8+ T cells in CD11c$^{\Delta raptor}$ mice after s.c. immunization, we assessed whether loss of raptor affected maturation, cytokine production and/or migration of sdLN migDCs in response to these immunizations. However, immunization with either PolyIC or CpG-B did not restore or further enhance the maturation of raptor-deficient migDCs *in vivo* (Figure 6A and S5A-B). Little IL-12p40/p70 production by migDCs was measured *ex vivo* following immunization *in vivo* (Figure S5C) and also the IL-12 production by migDCs from naïve CD11c^{WT} and CD11c$^{\Delta raptor}$ mice that were stimulated *ex vivo* with several TLR ligands was comparable (Figure 6B and S5D). No differences were found in the frequencies and numbers of Fluorescein isothiocyanate (FITC)+ skin migratory cDC1s and cDC2s in draining inguinal LNs from CD11c$^{\Delta raptor}$ mice and their CD11c^{WT} littermates 24 hours after inflammatory FITC painting of the flank (Figure 6C). Moreover, 72h after FITC painting, frequencies, numbers and maturation of these cells were not affected by loss of raptor (Figure 6C and S5E), suggesting that longevity of activated migDCs and their maintenance of high costimulatory molecule expression is not differentially impacted between raptor competent and raptor-deficient

cells. More importantly, this also suggests that CD11c-expressing cells other than migDCs may underlie the observed potentiated CD8+ T cell priming in CD11c$^{\Delta raptor}$ mice after s.c. immunization.

In the light of these findings, we turned our attention to Langerhans cells (LCs), which are another important group of professional APCs in the skin, that have migratory, T helper cell priming and CTL priming capacity [31]. Notably, LCs also express high levels of CD11c and may therefore be affected in this model. In line with work showing that LCs depend on mTORC1 signalling for their survival [16], we found that deletion of raptor in CD11c-expressing cells decreased steady state phosphorylation of ribosomal protein S6 in LCs from sdLNs (Figure S6A). This resulted in CD24+CD326+XCR1- LCs (Figure S6B) to be strongly reduced in frequency within the migratory APC gate (Figure 4A and S6C). However, due to the overall increased migratory APC pool size (Figure 4A,C) the total number of LCs in sdLNs was not different between CD11c^{WT} and CD11c$^{\Delta raptor}$ mice (Figure S6C). Moreover, the migratory capacity of LCs was intact after loss of raptor (Figure 6D). Loss of raptor decreased 2-NBDG uptake by LCs (Figure S6D) without affecting mitochondrial mass (Figure S6E), mitochondrial membrane potential (Figure S6E) in steady state conditions. Immunologically, a higher surface expression of costimulatory markers CD70 and CD80 could be observed on LCs from CD11c$^{\Delta raptor}$ mice compared to LCs from CD11c^{WT} mice after s.c. immunization with either PolyIC or CpG-B (Figure 6E and S5B). Moreover, these raptor-deficient LCs showed an approximately 2-fold higher production of IL-12 (Figure 6F and S5D). The production of IL-12 after stimulation with LPS was, however, not affected (Figure 6F). In line with this, s.c. immunization with LPS+OVA did, in contrast to immunizations with PolyIC or CpG (Figure 5), not result in enhanced IFNγ production by CD8+ T cells (Figure S6F,G). Finally, the reduced MHCI expression under steady state conditions by raptor-deficient LCs was restored to WT levels after TLR stimulation (Figure 6E). Correspondingly, cross presentation of soluble OVA SLP antigen was, in contrast to migDC1s, not significantly compromised in LCs from CD11c$^{\Delta raptor}$ mice (Figure 6G). This was associated with increased expression of autophagy marker LC3 in raptor-deficient LCs, but not in migDCs, relative to their raptor sufficient counterparts (Figure 6H-I). Taken together, these findings in the LC compartment may explain the enhanced CD8+ T cell response in CD11c$^{\Delta raptor}$ mice after s.c. immunization.

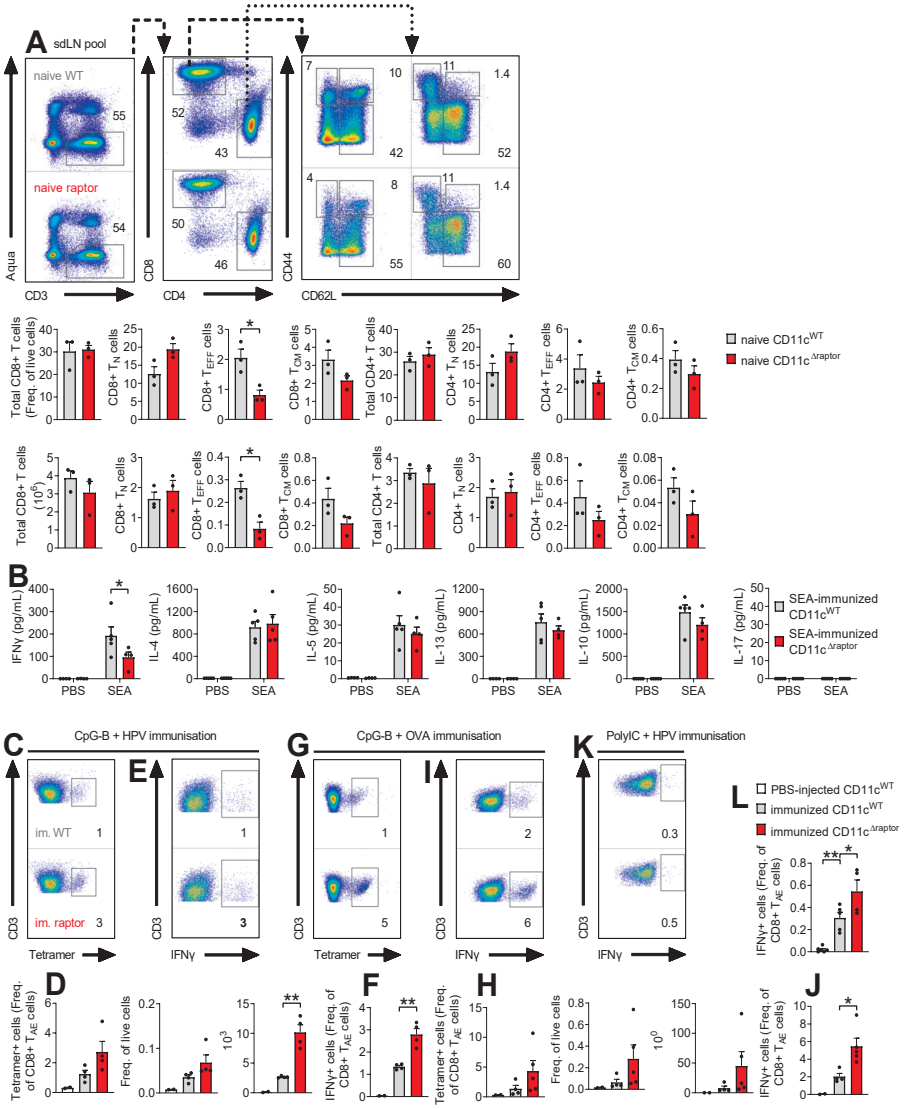
A
sdLN pool
naive WT
naive raptor
Aqua
CD3
CD8
CD4
CD44
CD62L
naive CD11c^WT
naive CD11c^Δraptor
B
IFNγ (pg/mL)
IL-4 (pg/mL)
IL-5 (pg/mL)
IL-13 (pg/mL)
IL-10 (pg/mL)
IL-17 (pg/mL)
PBS
SEA
SEA-immunized CD11c^WT
SEA-immunized CD11c^Δraptor
C
CpG-B + HPV immunisation
im. WT
im. raptor
Tetramer
E
IFNγ
G
CpG-B + OVA immunisation
I
K
PolyIC + HPV immunisation
L
PBS-injected CD11c^WT
immunized CD11c^WT
immunized CD11c^Δraptor
D
F
H
J

Figure 5. mTORC1 signalling in CD11c-expressing cells limits CD8+ T cell priming following subcutaneous immunization but not Th2 polarization.

(A) On the top a gating strategy for T cell subsets in skin-draining lymph nodes (sdLNs; pool of brachial, axillary and inguinal LNs) as shown in Figure 2A. Frequencies and numbers of splenic T cells are enumerated on the bottom. (B) $CD11c^{WT}$ and $CD11c^{\Delta raptor}$ mice were immunized with *S. mansoni* soluble egg antigens (SEA) by s.c. footpad injection and draining popLNs were collected 7 days later. popLN single cell suspensions were put into culture for 3 days with or without SEA. Supernatants were harvested and analysed for indicated cytokines by cytokine bead array. (C-F) Mice were immunized with HPV SLP and 25 µg of CpG-B by s.c. tailbase injection and T cell responses in draining inguinal lymph nodes (ingLNs) were analysed 7 days later by flow cytometry. (C,D) Representative histograms, frequencies and numbers of E7-specific CD8+ TAE cells based on D^bE7-tetramer staining as analysed by flow cytometry. (E,F) IngLN cells were stimulated with E7-SLP in the presence of Brefeldin A and analysed for HPV-specific IFNγ production by CD8+ TAE cells using flow cytometry. (G-J) Mice were immunized with OVA and 25 µg of CpG-B by s.c. footpad injection and T cell responses in draining popLNs were analysed 7 days later by flow cytometry. (G,H) Representative histograms, frequencies and numbers of OVA-specific CD8+ TAE cells based on K^bOVA-tetramer staining as analysed by flow cytometry. (I,J) popLN cells were stimulated with SIINFEKL in the presence of Brefeldin A and analysed for OVA-specific IFNγ production by CD8+ TAE cells using flow cytometry. (K,L) Mice were immunized with HPV and 25 µg of PolyIC by s.c. tailbase injection and T cell responses in draining ingLNs were analysed 7 days later by flow cytometry. ingLN cells were stimulated with E7-SLP in the presence of Brefeldin A and analysed for E7-specific IFNγ production by CD8+ TAE cells using flow cytometry. Data are from 1 experiment using 3 mice per group (A), 1 experiment using 4-5 mice per group (B), 1 experiment using 2-4 mice per group (C-F), 1 experiment using 2-5 mice per group (G-J) or 1 experiment using 2 lymph nodes from 2-3 mice per group (K-L). Data shown as mean ± SEM; $*p < 0.05$, $**p < 0.01$ when comparing samples between $CD11c^{WT}$ and $CD11c^{\Delta raptor}$ mice.

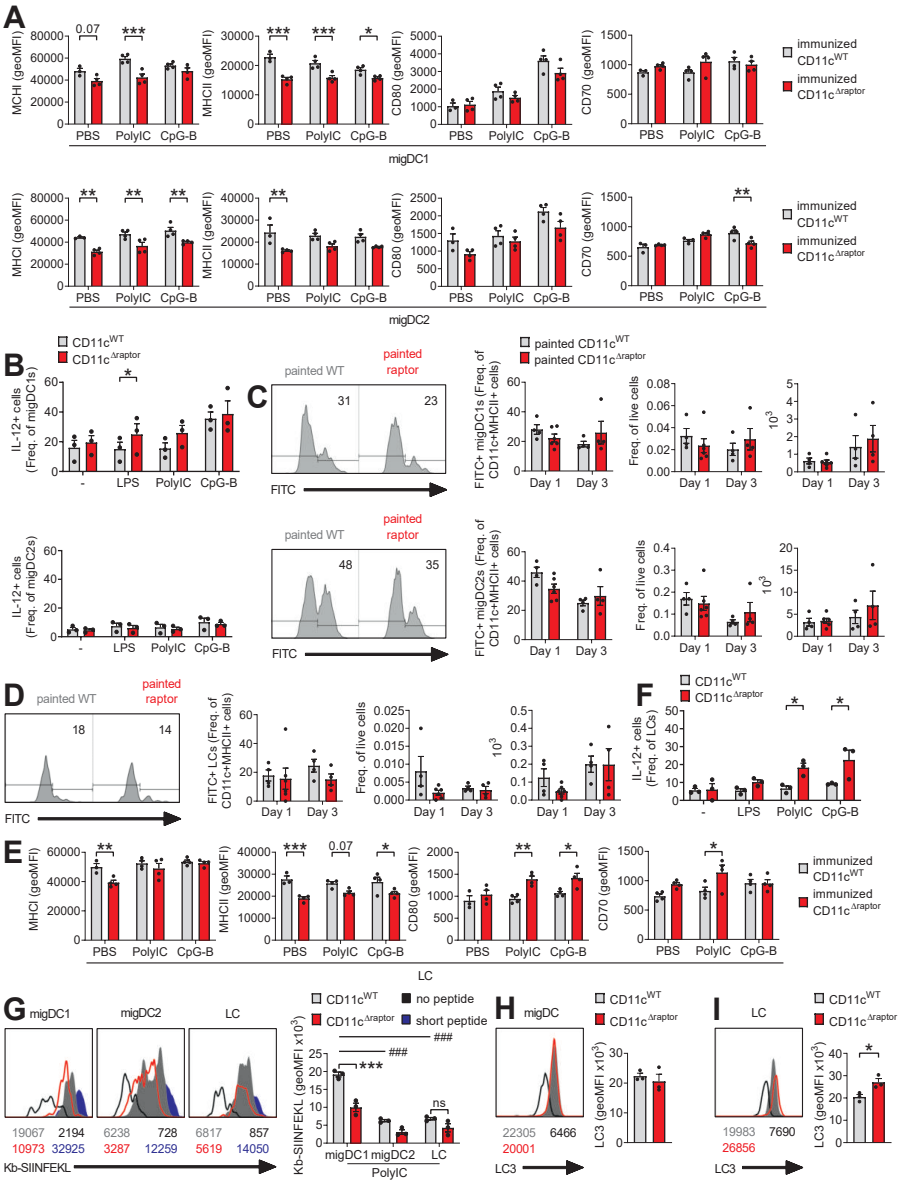
A
MCHI (geoMFI)
MHCII (geoMFI)
CD80 (geoMFI)
CD70 (geoMFI)
PBS
PolyIC
CpG-B
migDC1
migDC2
immunized CD11c^WT
immunized CD11c^Δraptor
B
CD11c^WT
CD11c^Δraptor
IL-12+ cells (Freq. of migDC1s)
IL-12+ cells (Freq. of migDC2s)
LPS
C
painted WT
painted raptor
FITC
painted CD11c^WT
painted CD11c^Δraptor
FITC+ migDC1s (Freq. of CD11c+MHCII+ cells)
FITC+ migDC2s (Freq. of CD11c+MHCII+ cells)
Freq. of live cells
Day 1
Day 3
D
FITC+ LCs (Freq. of CD11c+MHCII+ cells)
E
LC
F
IL-12+ cells (Freq. of LCs)
G
migDC1
migDC2
LC
Kb-SIINFEKL
no peptide
short peptide
Kb-SIINFEKL (geoMFI x10^3)
H
migDC
LC3
LC3 (geoMFI x10^3)
I
LC

Figure 6. mTORC1 signalling supports activation of migratory skin DCs but constrains activation of Langerhans Cells in response to subcutaneous immunization.

(A,E) CD11c^{WT} and CD11c$^{\Delta raptor}$ mice were immunized with either 25 µg of CpG-B or 25 µg of PolyIC by s.c. tailbase injection and (A) migDC1 and migDC2, and (E) LC maturation in draining inguinal lymph nodes (ingLNs) was analysed 24 hours later by flow cytometry. Representative histograms are in Figure S8B. (B,F) IngLN cells from naïve WT and CD11c$^{\Delta raptor}$ mice were stimulated with either 10 µg/mL PolyIC or 5 µg/mL CpG-B and all in the presence of Brefeldin A and analysed for production of IL-12p40/p70 by (B) migDC1s and migDC2s, and (H) LCs using flow cytometry. Representative histograms are in Figure S8C. (C,D) Mice were painted on their flank with inflammatory FITC paint and FITC+ migAPC migration was analysed on the indicated days by flow cytometry. (G) Flow cytometry-based analysis of cross presentation in sdLN migAPCs from CD11c^{WT} mice in grey, CD11c$^{\Delta raptor}$ mice in red, a no antigen negative control in black and a SIINFEKL positive control in blue. (H-I) Flow cytometry-based analysis of the autophagy marker Light Chain 3 (LC3) in sdLN migDCs (H) and LCs (I) from WT mice in grey CD11c$^{\Delta raptor}$ mice in red and a fluorescence minus one (FMO; no primary antibody) control in black. Data are from 1 experiment using 2 lymph nodes from 2 mice per group (A,E), 3 experiments using 1 mouse per group (B,F), 1 out of 2 representative experiments using 4-6 mice per group (C-D) or 1 experiment using 3 mice (G-I). Data shown as mean ± SEM; *p < 0.05, **p < 0.01, ***p < 0.001 when comparing samples between CD11c^{WT} and CD11c$^{\Delta raptor}$ mice; ###p < 0.001 when comparing populations within CD11c^{WT} mice.

Discussion

In the present study we aimed to determine how mTORC1 regulates DC metabolism and their T cell priming capacity *in vivo*. We show that the metabolic and immunological phenotype of professional APCs are differently affected by loss of mTORC1 signalling depending on their origin and location. Apart from compromised MHCI expression, homeostasis and activation of splenic cDCs was only minimally affected by deletion of raptor. On the other hand, raptor deficiency resulted in a greater abundance of migDCs in skin-draining LNs with a strongly reduced maturation profile, with the notable exception of LCs which showed increased expression of the costimulatory molecules and IL-12. These latter findings were associated with a potentiated ability of CD11c$^{\Delta raptor}$ mice to mount CD8 T cell responses following s.c. immunization. Together, these data highlight distinct effects of mTORC1 signalling inhibition on different APC subsets and may suggest that mTORC1 acts as a negative regulator of CD8 T cell priming selectively in LCs.

We found that splenic CD8+ cDC1s display higher uptake of the fluorescent glucose analogue 2-NBDG, and increased mitochondrial mass and membrane potential than splenic CD11b+ cDC2s. This is in line with a recent study that reported splenic CD8+ cDC1s to have higher mitochondrial respiration, glycolytic

flux, mitochondrial mass, and membrane potential than their CD8- counterpart [18]. This unique metabolic profile of splenic cDC1s was reported to depend on the Hippo pathway kinases Mst1 and Mst2 and was important for their function, which was illustrated by the fact that these DCs were much more sensitive to metabolic inhibitors such as metformin and 2-deoxyglucose than cDC2s [18]. We now report that also skin migratory cDC1s have relative high 2-NBDG uptake, mitochondrial mass and membrane potential, although the 2-NBDG uptake was similarly high in migDC1s and migDC2s. Consistent with a well described role for mTORC1 signalling in supporting glycolysis, mitochondrial biogenesis and preventing mitophagy in myeloid cells [7], 2-NBDG uptake and mitochondrial mass were reduced following loss of mTORC1 signalling. Interestingly, the former occurred specifically in splenic cDC1s while the latter happened explicitly in skin migDC1. How mTORC1 differentially affects the metabolism of DCs at different locations is currently unclear, but is likely to be influenced by local nutrient and growth factor availability which both are important determinants of mTORC1 activity.

Moreover, we found that raptor-deficient cDCs show a consistent reduction in MHCI surface expression at steady state conditions, while homeostasis, migration, costimulatory molecule expression and cytokine production are minimally affected. Although an important role for mTORC1 in the processing and presentation of antigens in the context of MHCII has been well established [3, 32], its role in antigen presentation in the context of MHCI is less well-defined. Stable MHCI surface expression is dependent on the transcription of MHCI and the availability of high affinity peptides, which under steady state are commonly derived from proteasome mediated degradation of cytosolic proteins [33]. The synthesis of these proteins [34] and the expression and activity of the proteasome [35] can be positively regulated by active mTORC1 signalling. Treatment of tumour cells with rapamycin indeed reduced the intracellular peptide pool and consequently the surface MHCI expression [34]. Additionally, mTORC1 inhibition is well known to promote autophagy which can reduce MHCI surface levels by mediating their degradation following endocytosis [36]. Such studies might provide an explanation for the reduced surface expression of MHCI on raptor-deficient DCs at steady state. Lower baseline MHCI expression on raptor-deficient DCs did not however translate into an impaired ability of $CD11c^{\Delta raptor}$ mice to mount CD8+ T cell responses to foreign antigens. This was apparent during both systemic (listeria infection) and local (s.c. immunization) immunological challenge. In fact, antigen-specific CD8+ T cell responses in $CD11c^{\Delta raptor}$ mice were even potentiated following s.c. immunization. While our data suggest that the latter observation - as discussed in more detail below – may stem from alterations in skin-resident LC function, the intact CD8+ T cell priming after listeria infection is likely to have a different basis. *L.*

monocytogenes primarily infects splenic macrophages and liver Kupffer cells. However, cDC1s are also directly infected and serve as a critical entry point to establish infection [37]. Following internalization, the bacteria can escape from phagosomes and access the host cytosol for replication. Hence, it has been shown that listeria-derived antigens from both exogenous/vacuolar and cytosolic origin can be presented in MHCI, via cross and direct presentation, respectively [23, 38]. Our observation that cross-presentation is not enhanced in raptor-deficient splenic cDC1s, might indicate that instead presentation of cytosolic listeria-derived antigens is enhanced. mTORC1 inhibition is well known to promote autophagy, a process that has been shown to be activated as a host protective mechanism to promote breakdown of intracellular bacteria [10], including listeria [39], and to facilitate generation of peptides for presentation on MHCI [40]. Further studies are required to determine whether enhanced presentation of listeria-derived antigens, as a consequence of increased autophagy, can compensate for overall lower MHCI expression and explain the uncompromised ability of $CD11c^{\Delta raptor}$ mice to mount antigen-specific CD8+ T cell responses following listeria infection.

Other aspects of DC biology - including longevity, the magnitude and duration of expression of costimulatory markers, cytokine expression and migration - that could potentially explain the differences in CD8+ T cell phenotype between $CD11c^{WT}$ and $CD11c^{\Delta raptor}$ mice, were not substantially different between TLR-stimulated DCs from $CD11c^{WT}$ and $CD11c^{\Delta raptor}$ mice both *in vivo* and *ex vivo*. This is at odds with *in vitro* studies showing that TLR-activated GMDCs display increased mitochondrial respiration, survival and duration of costimulatory molecule expression after treatment with rapamycin, which translated into an enhanced CD8+ T cell priming capacity following adoptive transfer *in vivo* [8-10]. This may in part be explained by different biological consequences of long-term deletion versus acute pharmacological inhibition. In addition, one well known difference between TLR-activated GMDCs and cDCs is that GMDCs, but not cDCs, express inducible nitric oxide (NO) synthase (iNOS) and produces NO in an mTOR-dependent manner, while the latter does not [14]. NO has been shown to poison mitochondrial respiration of GMDCs in an autocrine manner [12] and in line with this, beneficial effects of mTOR inhibition on GMDC immunogenicity were reported as secondary to reduced iNOS expression and NO production [13, 19]. This likely explains why loss of mTORC1 signalling in cDCs had less effect on these parameters. Consistent with a lack of clear immunological differences between splenic cDC1s from $CD11c^{WT}$ and $CD11c^{\Delta raptor}$ mice, we found that raptor competent and raptor-deficient PolyIC-activated splenic cDC1s were equally capable of inducing antigen-specific CD8+ T cell responses after adoptive transfer *in vivo*.

In search for an alternative explanation for the potentiated antigen-specific CD8+ T cell response following s.c. immunization in CD11c$^{\Delta raptor}$ mice, we found that loss of raptor in CD11c-expressing cells selectively augmented the activation of LCs reflected by increased expression of CD80, CD70 and IL-12 following immunization with either PolyIC or CpG. In addition, we observed that LC frequencies, but not total numbers, were significantly reduced in sdLNs. Our findings are largely consistent with earlier studies showing that LCs are critically dependent on raptor for their homeostasis in skin epidermis and dermis, but their frequencies are less negatively affected by raptor deficiency in draining lymph nodes [16]. In addition, LC-specific deletion of p14, a protein required for mTORC1 activation, resulted in stronger activation as determined by CD86 and MHCII expression [41]. However, the consequences of these phenotypes for *in vivo* T cell priming were not evaluated in these studies. Another interesting observation was that TLR stimulation recovered the defect in MHCI expression by LCs from CD11c$^{\Delta raptor}$ mice, which was still reduced on cDCs from those same LNs. Likewise, in contrast to migratory cDCs lacking raptor, the cross-presentation ability of LCs was not compromised. This was associated with increased expression of LC3, marking enhanced autophagic activity in raptor-deficient LCs. Since autophagy can promote cross-presentation, it is tempting to speculate that the increased activation of autophagy due to loss of mTORC1 signalling may help to restore MHCI surface expression on LCs by facilitating cross-presentation. This uncompromised MHCI expression by raptor-deficient LCs, together with increased expression of IL-12 and costimulation, in particular provided by CD70 - signals which are known to underpin CTL priming and IFNγ-production [25, 42] - strongly point towards a central role for LCs in driving the potentiated antigen-specific CD8+ T cell response following s.c. immunization in CD11c$^{\Delta raptor}$ mice. Murine LCs are generally considered to have inferior cross-presenting potential compared to murine cDC1s and human LCs [31] and this is reflected in their transcriptome [43]. Moreover, they have also been shown dispensable for the generation of CD8+ CTLs in response to infections [31], such as herpes simplex virus [44], *Candida albicans* [45] and pox vaccinia virus [46]. Nonetheless, this does not exclude the possibility that the augmented activation profile of LCs from CD11c$^{\Delta raptor}$ mice can directly contribute to the observed enhanced CD8+ T cell priming *in vivo*. This would be supported by our observations that IL-12 production by LCs was increased after *ex vivo* stimulation with ligands for TLR3 and TLR9 but not TLR4, which was mirrored by higher frequencies of antigen-specific CD8+ T cell responses following immunization with ligands for TLR3 and TLR9 as adjuvant but not TLR4. Together, our data support the idea that LCs play a key role in the potentiated antigen-specific CD8+ T cell response in CD11c$^{\Delta raptor}$ mice following s.c. immunization. An intriguing question that remains to be answered is why loss of raptor has such strikingly divergent effects on LC and

cDC biology. Possibly the potentiating effects of loss of raptor selectively on LC activation, but not cDCs, could be explained by studies showing that beta-catenin, which is constitutively active and required for LC differentiation but dispensable for dermal DC differentiation [47], has anti-inflammatory effects on DCs through activation of mTORC1 [26]. This would render LCs particularly sensitive to effects of mTORC1 inhibition. Further studies are warranted to better understand the differential effects mTORC1 signalling on DCs versus LCs.

Our observations highlight that pharmacological inhibition of mTORC1 may be a viable means to boost cellular immunity following vaccination. Interestingly, since LCs have also been reported to promote CD4+ T follicular helper cell differentiation, germinal center formation and humoral responses in a variety of settings [48-52], not only cellular, but also humoral immune responses may benefit from local mTORC1 inhibition in response to vaccination and clearly warrants further study. In summary, we provide evidence for distinct effects of mTORC1 signalling in different APC subsets plays on their ability to prime cytotoxic T cell responses, with selectively an inhibitory role for mTORC1 in this process in LCs, which may have implications for vaccination practices.

References

1. Kapsenberg, M.L., *Dendritic-cell control of pathogen-driven T-cell polarization.* Nat Rev Immunol, 2003. **3**(12): p. 984-93.
2. Eisenbarth, S.C., *Dendritic cell subsets in T cell programming: location dictates function.* Nat Rev Immunol, 2019. **19**(2): p. 89-103.
3. Patente, T.A., L.R. Pelgrom, and B. Everts, *Dendritic cells are what they eat: how their metabolism shapes T helper cell polarization.* Curr Opin Immunol, 2019. **58**: p. 16-23.
4. Saxton, R.A. and D.M. Sabatini, *mTOR Signaling in Growth, Metabolism, and Disease.* Cell, 2017. **168**(6): p. 960-976.
5. Jones, R.G. and E.J. Pearce, *MenTORing Immunity: mTOR Signaling in the Development and Function of Tissue-Resident Immune Cells.* Immunity, 2017. **46**(5): p. 730-742.
6. Snyder, J.P. and E. Amiel, *Regulation of Dendritic Cell Immune Function and Metabolism by Cellular Nutrient Sensor Mammalian Target of Rapamycin (mTOR).* Front Immunol, 2018. **9**: p. 3145.
7. Weichhart, T., M. Hengstschlager, and M. Linke, *Regulation of innate immune cell function by mTOR.* Nat Rev Immunol, 2015. **15**(10): p. 599-614.
8. Amiel, E., et al., *Inhibition of mechanistic target of rapamycin promotes dendritic cell activation and enhances therapeutic autologous vaccination in mice.* J Immunol, 2012. **189**(5): p. 2151-8.
9. Jagannath, C. and P. Bakhru, *Rapamycin-induced enhancement of vaccine efficacy in mice.* Methods Mol Biol, 2012. **821**: p. 295-303.
10. Jagannath, C., et al., *Autophagy enhances the efficacy of BCG vaccine by increasing peptide presentation in mouse dendritic cells.* Nat Med, 2009. **15**(3): p. 267-76.
11. Amiel, E., et al., *Mechanistic target of rapamycin inhibition extends cellular lifespan in dendritic cells by preserving mitochondrial function.* J Immunol, 2014. **193**(6): p. 2821-30.
12. Everts, B., et al., *Commitment to glycolysis sustains survival of NO-producing inflammatory dendritic cells.* Blood, 2012. **120**(7): p. 1422-31.
13. Lawless, S.J., et al., *Glucose represses dendritic cell-induced T cell responses.* Nat Commun, 2017. **8**: p. 15620.
14. Thwe, P.M. and E. Amiel, *The role of nitric oxide in metabolic regulation of Dendritic cell immune function.* Cancer Lett, 2018. **412**: p. 236-242.
15. Sinclair, C., et al., *mTOR regulates metabolic adaptation of APCs in the lung and controls the outcome of allergic inflammation.* Science, 2017.
16. Kellersch, B. and T. Brocker, *Langerhans cell homeostasis in mice is dependent on mTORC1 but not mTORC2 function.* Blood, 2013. **121**(2): p. 298-307.
17. Ohtani, M., et al., *Cutting edge: mTORC1 in intestinal CD11c+ CD11b+ dendritic cells regulates intestinal homeostasis by promoting IL-10 production.* J Immunol, 2012. **188**(10): p. 4736-40.
18. Du, X., et al., *Hippo/Mst signalling couples metabolic state and immune function of CD8alpha(+) dendritic cells.* Nature, 2018.

19. Everts, B., et al., *TLR-driven early glycolytic reprogramming via the kinases TBK1-IKKvarepsilon supports the anabolic demands of dendritic cell activation.* Nat Immunol, 2014. **15**(4): p. 323-32.
20. Guak, H., et al., *Glycolytic metabolism is essential for CCR7 oligomerization and dendritic cell migration.* Nat Commun, 2018. **9**(1): p. 2463.
21. Thwe, P.M., et al., *Cell-Intrinsic Glycogen Metabolism Supports Early Glycolytic Reprogramming Required for Dendritic Cell Immune Responses.* Cell Metab, 2017. **26**(3): p. 558-567.e5.
22. Chávez-Arroyo, A. and D.A. Portnoy, *Why is Listeria monocytogenes such a potent inducer of CD8+ T-cells?* Cell Microbiol, 2020. **22**(4): p. e13175.
23. Reinicke, A.T., et al., *Dendritic cell cross-priming is essential for immune responses to Listeria monocytogenes.* PLoS One, 2009. **4**(10): p. e7210.
24. Mintern, J.D., et al., *Differential use of autophagy by primary dendritic cells specialized in cross-presentation.* Autophagy, 2015. **11**(6): p. 906-17.
25. Mashayekhi, M., et al., *CD8α(+) dendritic cells are the critical source of interleukin-12 that controls acute infection by Toxoplasma gondii tachyzoites.* Immunity, 2011. **35**(2): p. 249-59.
26. Fu, C., et al., *beta-Catenin in dendritic cells exerts opposite functions in cross-priming and maintenance of CD8+ T cells through regulation of IL-10.* Proc Natl Acad Sci U S A, 2015. **112**(9): p. 2823-8.
27. van Panhuys, N., F. Klauschen, and R.N. Germain, *T-cell-receptor-dependent signal intensity dominantly controls CD4(+) T cell polarization In Vivo.* Immunity, 2014. **41**(1): p. 63-74.
28. Hussaarts, L., et al., *Rapamycin and omega-1: mTOR-dependent and -independent Th2 skewing by human dendritic cells.* Immunol Cell Biol, 2013. **91**(7): p. 486-9.
29. Pearce, E.J. and A.S. MacDonald, *The immunobiology of schistosomiasis.* Nat Rev Immunol, 2002. **2**(7): p. 499-511.
30. Maynard, S.K., et al., *Vaccination with synthetic long peptide formulated with CpG in an oil-in-water emulsion induces robust E7-specific CD8 T cell responses and TC-1 tumor eradication.* BMC Cancer, 2019. **19**(1): p. 540.
31. Kaplan, D.H., *Ontogeny and function of murine epidermal Langerhans cells.* Nat Immunol, 2017. **18**(10): p. 1068-1075.
32. Sukhbaatar, N., M. Hengstschlager, and T. Weichhart, *mTOR-Mediated Regulation of Dendritic Cell Differentiation and Function.* Trends Immunol, 2016. **37**(11): p. 778-789.
33. Williams, A., C.A. Peh, and T. Elliott, *The cell biology of MHC class I antigen presentation.* Tissue Antigens, 2002. **59**(1): p. 3-17.
34. Reits, E.A., et al., *Radiation modulates the peptide repertoire, enhances MHC class I expression, and induces successful antitumor immunotherapy.* J Exp Med, 2006. **203**(5): p. 1259-71.
35. Zhang, Y., et al., *Coordinated regulation of protein synthesis and degradation by mTORC1.* Nature, 2014. **513**(7518): p. 440-3.
36. Loi, M., et al., *Macroautophagy Proteins Control MHC Class I Levels on Dendritic Cells and Shape Anti-viral CD8(+) T Cell Responses.* Cell Rep, 2016. **15**(5): p. 1076-1087.

37. Edelson, B.T., et al., *CD8α(+) dendritic cells are an obligate cellular entry point for productive infection by Listeria monocytogenes.* Immunity, 2011. **35**(2): p. 236-48.
38. Villanueva, M.S., A.J. Sijts, and E.G. Pamer, *Listeriolysin is processed efficiently into an MHC class I-associated epitope in Listeria monocytogenes-infected cells.* J Immunol, 1995. **155**(11): p. 5227-33.
39. Riebisch, A.K., et al., *Autophagy-A Story of Bacteria Interfering with the Host Cell Degradation Machinery.* Pathogens, 2021. **10**(2).
40. Fiegl, D., et al., *Amphisomal route of MHC class I cross-presentation in bacteria-infected dendritic cells.* J Immunol, 2013. **190**(6): p. 2791-806.
41. Sparber, F., et al., *The late endosomal adaptor molecule p14 (LAMTOR2) represents a novel regulator of Langerhans cell homeostasis.* Blood, 2014. **123**(2): p. 217-27.
42. Rowley, T.F. and A. Al-Shamkhani, *Stimulation by soluble CD70 promotes strong primary and secondary CD8+ cytotoxic T cell responses in vivo.* J Immunol, 2004. **172**(10): p. 6039-46.
43. Artyomov, M.N., et al., *Modular expression analysis reveals functional conservation between human Langerhans cells and mouse cross-priming dendritic cells.* J Exp Med, 2015. **212**(5): p. 743-57.
44. Allan, R.S., et al., *Epidermal viral immunity induced by CD8alpha+ dendritic cells but not by Langerhans cells.* Science, 2003. **301**(5641): p. 1925-8.
45. Igyártó, B.Z., et al., *Skin-resident murine dendritic cell subsets promote distinct and opposing antigen-specific T helper cell responses.* Immunity, 2011. **35**(2): p. 260-72.
46. Seneschal, J., X. Jiang, and T.S. Kupper, *Langerin+ dermal DC, but not Langerhans cells, are required for effective CD8-mediated immune responses after skin scarification with vaccinia virus.* J Invest Dermatol, 2014. **134**(3): p. 686-694.
47. Yasmin, N., et al., *β-Catenin promotes the differentiation of epidermal Langerhans dendritic cells.* J Invest Dermatol, 2013. **133**(5): p. 1250-9.
48. Bouteau, A., et al., *DC Subsets Regulate Humoral Immune Responses by Supporting the Differentiation of Distinct Tfh Cells.* Front Immunol, 2019. **10**: p. 1134.
49. Levin, C., et al., *Critical Role for Skin-Derived Migratory DCs and Langerhans Cells in T(FH) and GC Responses after Intradermal Immunization.* J Invest Dermatol, 2017. **137**(9): p. 1905-1913.
50. Marschall, P., et al., *Dual function of Langerhans cells in skin TSLP-promoted T(FH) differentiation in mouse atopic dermatitis.* J Allergy Clin Immunol, 2020.
51. Yao, C., et al., *Skin dendritic cells induce follicular helper T cells and protective humoral immune responses.* J Allergy Clin Immunol, 2015. **136**(5): p. 1387-97.e1-7.
52. Zimara, N., et al., *Langerhans cells promote early germinal center formation in response to Leishmania-derived cutaneous antigens.* Eur J Immunol, 2014. **44**(10): p. 2955-67.
53. Poussin, M.A. and H. Goldfine, *Evidence for the involvement of ActA in maturation of the Listeria monocytogenes phagosome.* Cell Res, 2010. **20**(1): p. 109-12.
54. Pelgrom, L.R., et al., *LKB1 expressed in dendritic cells governs the development and expansion of thymus-derived regulatory T cells.* Cell Res, 2019. **29**(5): p. 406-419.
55. Everts, B., et al., *Omega-1, a glycoprotein secreted by Schistosoma mansoni eggs, drives Th2 responses.* J Exp Med, 2009. **206**(8): p. 1673-80.

Materials and methods

Mice

Itgax-cre Rptor-fl/fl (CD11c-cre raptor-fl/fl or CD11c$^{\Delta raptor}$ mice), transgenic with OVA specific CD4 T cells (OT-II), transgenic with OVA specific CD8+ T cells (OT-I) and wild type (WT) mice, both male and female and all on a C57BL/6J background, were bred under SPF conditions at the Leiden University Medical Center (LUMC), Leiden, The Netherlands. Mice were culled through cervical dislocation. Anaesthesia with isoflurane was used for *L. monocytogenes* infection and ketamine with either dexdomitor or xylazine was used for *S. mansoni* infection. Animal experiments were performed when the mice were between 8-16 weeks old. Animal experiments were performed in accordance with local government regulations, EU Directive 2010/63EU and Recommendation 2007/526/EC regarding the protection of animals used for experimental and other scientific purposes, as well as approved by the Dutch Central Authority for Scientific Procedures on Animals (CCD). Animal license number AVD116002015253.

Digestion of murine tissues

Lymphoid organs were collected in 500 µL of no additives media (naRPMI = RPMI-1640 supplemented with GlutaMAX™ [#61870-010 or alternatively 61870036, Gibco, Bleiswijk, The Netherlands], which should contain Ca^{2+} for the collagenase) in a plate and mechanically disrupted using the back-end of a syringe before addition of 50 µL of a digestion media (dRPMI = naRPMI supplemented with 11x collagenase D (#11088866001, Roche, Woerden, The Netherlands; end concentration of 1 mg/mL) and 11x DNase I (#D4263, Sigma, Zwijndrecht, The Netherlands; end concentration of 2000 U/mL) for 20 minutes at 37°C and 5% CO_2. Single cell suspensions were filtered after digestion with a 100 µm sterile filter (#352360, BD Biosciences, Vianen, The Netherlands) before counting in complete RMPI (cRPMI = naRPMI supplemented with 10% heat-inactivated FCS [#S-FBS-EU-015, Serana, Pessin, Germany], 50 µM β-mercaptoethanol [#M6250, Sigma], 100 U/mL penicillin [#16128286, Eureco-pharma, Ridderkerk, The Netherlands; purchased inside the LUMC] and 100 µg/mL streptomycin [#S9137, Sigma]). Spleens were subjected to red blood cell lysis (inhouse; 0.15 M NH4Cl, 1 mM KHCO3, 0.1 mM EDTA [#15575-038, Thermo, Waltham, Massachusetts, United States] in ddH_20) for 2 minutes at room temperature before counting.

Generation of bone marrow-derived GMDCs

BM cells were flushed from mouse femurs and tibia and plated in 'Nunc™ Cell-Culture Treated 6-well plate' wells (#140675, Thermo; approximate growth area of 9.5 cm^2) at a seeding density of 2x10^6 cells in a volume of 3 mL of complete RPMI for BM cells (cRPMI-BM = RPMI-1640 supplemented with GlutaMAX™ and also 5% FCS, 50 µM β-mercaptoethanol, 100 U/mL penicillin and 100 µg/mL streptomycin was put in) to which 20 ng/mL of recombinant GM-CSF (#315-03, PeproTech, Hamburg, Germany) was added. Media was refreshed on day 3-4 by adding 3 mL cRPMI-BM with 40 ng/mL GM-CSF and on day 7 by first removing 3 mL of supernatant and then adding 3 mL cRPMI-BM with 40 ng/mL GM-CSF. Semi-adherent cells were harvested for various assays on day 8. Alternatively, semi-adherent cells were collected on day 7 and seeded in a flat bottom 96-well plate (Nunc™; #167008, Thermo) at 1x10^5 cells in a volume of 200 µL of fresh cRPMI-BM with 20 ng/mL GM-CSF and rested overnight. Minimum rest time after transfer of GMDCs was 2-3 hours.

Flow cytometry

In general, single cell suspensions underwent viability staining for 20 minutes at room temperature using the LIVE/DEAD™ Fixable Aqua Dead Cell Stain Kit (#L34957, Thermo; 1:400 in PBS [from LUMC pharmacy; Braun, Zeist, The Netherlands) and fixation for 15 minutes at room temperature using 1.85% formaldehyde (F1635, Sigma) in PBS solution before surface staining with antibodies in an in-house cell separation buffer (= PBS supplemented with 0.5% BSA [fraction V, #10735086001, Roche, Woerden, The Netherlands] and 2 mM EDTA) for 30 minutes at 4 degrees Celsius. For detection of phosphorylated S6 on Ser235/236, single cell suspensions in cRPMI were returned to a cell incubator (37°C & 5% CO_2) for 1 hour after which 16% ultra-pure formaldehyde (#18814-20, Polysciences, Hirschberg an der Bergstraße, Germany) was added until the concentration reached 4% and the cells were left for 10 more minutes in the incubator to fix. For example, 67 µL of 16% ultra-pure formaldehyde was added to 200 µL of cell solution. Viability staining was not done before fixation to minimise changes in phosphorylation status. Single cell suspensions were first stained with anti-phosphorylated S6 in 1x Permeabilization Buffer (#00-8333-56, Thermo) for 1 hour at room before staining with other antibodies in the in-house cell separation buffer for 30 minutes at 4°C. For detection of mitochondrial mass and mitochondrial membrane potential, single cell suspensions were incubated with respectively 200 nM MitoTracker Green (#M7514, Invitrogen) or 200 nM TMRM (#T668, Thermo) in cRPMI for 30 minutes in a cell incubator. Subsequent viability and surface staining were done for 30 minutes on ice. No fixation occurred before running the samples. Uptake of 2-NBDG (N13195, Invitrogen) was done in a similar fashion but with 15 minutes of incubation. CD8+ T cells bearing antigen-specific T cell receptors were

quantified using in-house produced tetramers of MHCI:peptide complexes with SIINFEKL (K^bOVA-tetramer) or RAHYNIVTF (D^bE7-tetramer) as their respective epitopes. For detection of antigen-specific cytokine production by T cells, single cell suspensions in cRPMI were restimulated with either 1 µg/mL of SIINFEKL (in-house) or 1 µg/mL of RAHYNIVTF (in-house) in the presence of 10 µg/mL of Brefeldin A (#B7651, Sigma) for 4 hours in a cell incubator. For polyclonal restimulation, single cell suspensions were stimulated with both 0.1 µg/mL of PMA (#P-8139, Sigma) and 1 µg/mL of ionomycin (#I-0634, Sigma) in the presence of Brefeldin A. These single cell suspensions underwent intracellular cytokine staining (ICS) with antibodies in the 1x Permeabilization Buffer. For detection of IL-12 by DCs, single cell suspensions were stimulated with either 100 ng/mL of LPS, 10 µg/mL of PolyIC or 5 µg/mL of CpG-B (#TLRL-PELPS, #tlrl-1826-1 and #TLRL-PIC, respectively and all InvivoGen, Toulouse, France) and all in the presence of Brefeldin A for 5 hours in a cell incubator. Cross presentation was quantified by surface staining with an anti-Kb-SIINFEKL antibody after 3 hours of stimulation with OVA SLP (in house; 50 µg/mL for skin draining lymph node cells) in the presence of 10 µg/mL PolyIC. SIINFEKL (1 µg/mL) was used as positive MHCI loading control. All samples were run on a BD LSR II or FACSCanto II and analysed using FACS Diva 8 (all BD Biosciences) and FlowJo (Version 10, TreeStar, Meerhout, Belgium).

Antibodies

The antibodies used in this study can be found in supplementary table 1.

Western blotting

A million GMDCs were washed twice with PBS before being lysed in 150 µL of EBSB buffer (8% [w/v] glycerol, 3% [w/v] SDS and 100 mM Tris–HCl [pH 6.8]). Lysates were immediately boiled for 5 min and their protein content was determined using a BCA kit. Ten µg of protein per lain was separated by SDS-PAGE followed by transfer to a PVDF membrane. Membranes were blocked for 1 h at room temperature in TTBS buffer (20 mM Tris–HCl [pH 7.6], 137 mM NaCl, and 0.25% [v/v] Tween 20) containing 5% (w/v) fat free milk and incubated overnight with primary antibodies. The primary antibodies used were raptor (A300-506A clone; 1:1000; Bethyl Laboratories, Montgomery, Texas, United States) and beta-actin (AC-15 clone; 1:2000; Sigma). The membranes were then washed in TTBS buffer and incubated with horseradish peroxidase-conjugated secondary antibodies for 2 h at room temperature. After washing, blots were developed using an in-house enhanced chemiluminescence solution (10 mL of substrate [16.67 mL 3M Tris-HCl <pH 8.8>, 125 mg sodium luminol <#A4685, Sigma>, 155 µL H2O2 <#7047, Baker> and mQ up to 500 mL] with 10 µL of enhancer [11 mg coumaric acid <#C9008> in 10 mL of DMSO]).

Preparation of Listeria monocytogenes bacteria

Listeria monocytogenes bacteria were scraped from a glycerol stock and transferred to a 15 mL round bottom polysterene tube (#352051, Corning, Amsterdam, The Netherlands) with 3 mL of 'Brain Heart Infusion (BHI) Broth' (#37500, BD Biosciences) and incubated overnight at 37 degrees with the cap loose and the tube rotating at 200 rpm. The next day, 20 and 50 µL of bacteria solution was transferred to new tubes with broth and cultured for another 3 hours. The optical density (OD) was measured at 600 nm (OD600) using a spectrophotometer (#Ultrospec 100 pro, GE Healthcare, Hoevelaken, The Netherlands after takeover of Amersham Biosciences by GE Healthcare) and the concentration of bacteria solution was corrected until the OD600 value corresponded approximately to 1.2x10^8 colony forming units (CFU) per mL of broth, which was previously determined by titration. To make new glycerol stocks, 1 mL of the overnight cultured bacterial solution and 500 µL of pure glycerol were mixed well and stored at -80 degrees.

Listeria monocytogenes infection and challenge

Mice were infected with a live attenuated OVA-expressing *L. monocytogenes* strain deficient in actin assembly-inducing protein (Lm-dActA-OVA), which is required for escape from phagosomes and cell-to-cell spreading [53]. Bacteria were centrifuged at 2000 rpm for 10 minutes at 4 degrees and brought to 2.5x107 CFU per mL of PBS. Mice were sedated with isoflurane and infected by retro-orbital intravenous (i.v.) injection with 200 µL of bacteria in PBS (=5x106 CFU). The remaining bacteria were brought to 103 CFU per mL of PBS and 50 µL of this bacteria solution (=50 CFU) was plated on a 'BHI Agar Plate' (#255003, BD Biosciences) and incubated overnight at 37 degrees for control counting of colonies next day. Mice were culled 7 days later, and organs were processed as described above. Alternatively, 21 days after infection, mice were challenged with 5x104 OVA-expressing wild type bacteria (Lm-OVA) in 200 µL of PBS by retro-orbital i.v. injection and at day 24, mice were culled, and organs were processed as described above. Bacterial load in the organs was determined by taking 100 µL of a 5 mL single cell suspension in PBS and lysing this in 900 µL 0.1% Triton-X-100 (T8532, Sigma) in mQ (1:10 single cell suspension:0.1% Triton) and making further dilutions of 1:100 and 1:1000 before plating on a agar plate and overnight incubation at 37 degrees for control counting of colonies the next day.

In vivo cDC expansion, isolation, sorting and transfer
The *in vivo* expansion of cDCs using Flt3L-secreting B16 melanoma cells and their subsequent sorting, *ex vivo* conditioning and transfer into recipient mice to induce DC-specific T cell responses was done as described previously [54]. cDC1s were stimulated with 100 µg/mL of ovalbumin (OVA; #vac-pova-100, InvivoGen) and 10 µg/mL of PolyIC. 300.000 cells were transferred.

Preparation of Schistosoma mansoni soluble egg antigens
S. mansoni eggs were isolated and processed into a SEA preparation as described previously [55]. Protein concentration was determined using a bicinchoninic acid (BCA) protein assay kit (Pierce, #PIER23225). Endotoxin contamination was determined by a direct comparison of SEA batches to LPS in a TLR4-transfected Human Embryonic Kidney 293 (HEK) reporter cell line, in which IL-8 secretion by 5x108 HEK cells after stimulation with 10 µg of SEA is expected to be similar or less than after stimulation with 1-3 ng/mL of LPS.

Schistosoma mansoni acute infection
Mice were infected with *S. mansoni* (Puerto Rican strain; Naval Medical Research Institute) by 30 minutes of percutaneous exposure to 60 cercariae (or up to 100 cercariae) on shaved abdomen. Mice were culled 8 weeks later. Cercariae were kept at 30 cercariae per mL of store bought Barleduc water, which was kept very carefully at 31 degrees Celsius. Female mice were anesthetized by intraperitoneal (i.p) injection with 300 µL of 50 mg/kg bodyweight ketamine + 0.5 mg/kg bodyweight dexdomitor, while male mice were anesthetized with 50 mg/kg bodyweight ketamine + 10 mg/kg bodyweight xylazine. Female mice were assisted in waking up by i.p. injection with 150 µL of 0.4 mg/kg bodyweight antisedan. All injections were done using PBS and a 25G needle. All anaesthetics were bought at the LUMC pharmacy. Livers were processed like spleens except that single cell suspensions were centrifuged twice at 20 g for 10 minutes in PBS to remove hepatocytes before red blood cell lysis.

In vivo T cell priming and DC activation following immunization
For evaluation of T cell priming, mice were injected s.c. either with a) 5 µg of LPS together with 25 µg of OVA and emulsified in 40 µL of incomplete Freunds' adjuvant (IFA; #vac-ifa-10, InvivoGen) in the hind footpad, or b) 10-25 µg of CpG-B with OVA and in IFA in the footpad, or c) 25 µg of PolyIC with 100 µg of E7-SLP in 50 µL of PBS in the tailbase, or d) 25 µg of CpG-B with E7-SLP in PBS in the tailbase. Mice were culled 7 days later and draining popLNs were collected after footpad injection and draining ingLNs were collected after tailbase injection. For evaluation of DC activation, OVA- and E7-SLP were omitted and draining LNs were collected after 24 hours instead of 7 days.

Cytometric bead array
Cell culture supernatants were analysed for IFNγ, IL-4, IL-5, IL-10 and IL-13 secretion using a cytokine bead array (#I558296, #558298, #558302, #558300 and #558349 respectively and all BD Biosciences) on a flow cytometer as recommended by the manufacturer, but with both the beads and antibodies diluted 1:10 relative to the original recommendation.

FITC painting
Mice were painted with 20 µL of inflammatory FITC paint (5 mg/ml fluorescein isothiocyanate [#F3651, Sigma] in a 1:1 mix of dibutylphalate [#524980, Sigma] and acetone [#100014, Merck, Amsterdam, The Netherlands]) on shaved flanks and draining ingLNs were collected either 1 or 3 days later.

Quantification and statistical analysis
Statistical analysis as specified in figure legends were performed with Prism 9 (GraphPad software Inc., San Diego, California, United States). Graphs with 2 bars were analysed with the non-paired Student's t test, while graphs with more than 2 bars were analysed with the two-way unpaired analysis of variance (ANOVA) corrected for multiple comparisons using Sidak's multiple comparison test. Graphs with multiple time points were analysed with a simple linear regression. A p value < 0.05 was considered significant (*/# for $p < 0.05$, **/## for $p < 0.01$ and ***/### for $p < 0.001$).

Acknowledgements
This work was supported by an LUMC fellowship awarded to BE.

Author contributions
LP, TP, FO, LN, AO, AvdH, HvdZ and BE performed experiments. LP and BE analysed experiments. LP, RA and BE designed experiments. BE conceived and supervised the study and wrote the manuscript together with LP.

Conflict of interest
The authors declare that no competing financial interests exist in relation to the work described.

Supplemental figures

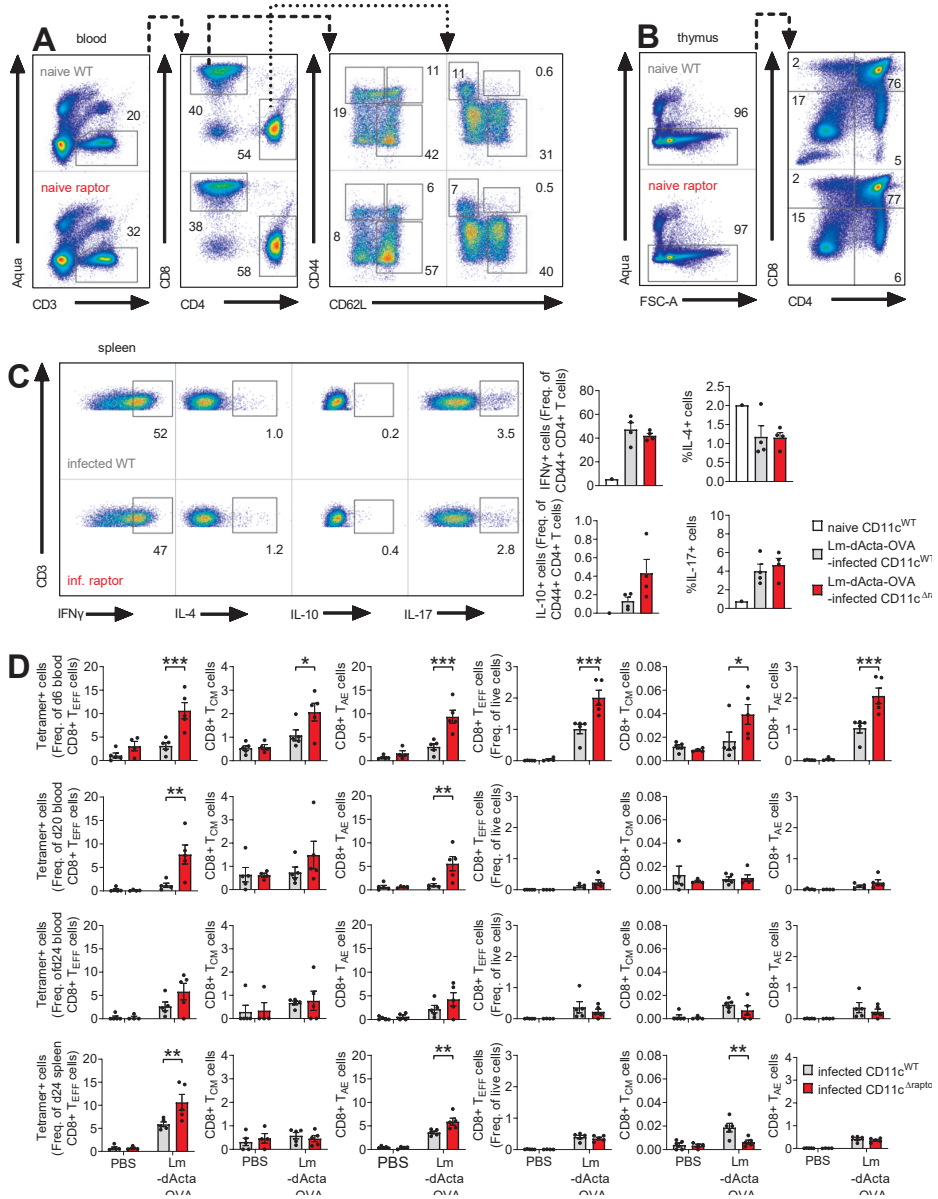

Figure S1.

(A) Gating strategy for T cell subsets in blood by sequential gating of intact cells (forward scatter area [FSC-A] versus side scatter area [SSC-A], not shown), singlets (FSC-A versus forward scatter height [FSC-H], not shown), live cells (Aqua- cells in panel 1), live T cells (CD3+ versus Aqua- cells in panel 1), total CD4 T cells (CD4+ versus CD8+ in panel 2) and total CD8+ T cells (CD4- versus CD8+ in panel 2), naïve CD8+ T cells (CD8+ TN; CD62L+ versus CD44- in panel 3) and effector CD8+ T cells (CD8+ TEFF; CD62L- versus CD44+ in panel 3) and central memory CD8+ T cells (CD8+ TCM; CD62L+ versus CD44+ in panel 3), and naïve CD4 T cells (CD4+ TN; CD62L+ versus CD44- in panel 4) and effector CD4 T cells (CD4+ TEFF; CD62L- versus CD44+ in panel 4) and central memory CD4+ T cells (CD4+ TCM; CD62L+ versus CD44+ in panel 4). Antigen-experienced T cells (TAE) are the sum of TEFF and TCM subsets. (B) Representative histograms of developing T cells in the thymus of naïve $CD11c^{WT}$ and $CD11c^{\Delta raptor}$ mice. (C) Splenocytes were stimulated with PMA/ionomycin the presence of Brefeldin A and analysed for production of indicated cytokines by CD4+ TAE cells using flow cytometry. (D) Mice were infected with 5x10^6 Lm-dActa-OVA by i.v. injection and challenged 21 days later with 5x10^4 Lm-OVA. Blood was drawn on day 6,20 and 24 and mice were culled on day 24 to take spleen. OVA-specific CD8+ T cells based on K^bOVA-tetramer staining as analysed by flow cytometry. Frequencies of OVA-specific T cell subsets as gated in S2A are enumerated. Data is from 1 experiment out 3 (which together are the same mice as Figure 2B-D) using 1-4 mice per group (C) or from 1 out of 2 representative experiments (same mice as Figure 2E) using 4-5 mice per group (D) and shown as mean ± SEM; *p < 0.05, **p < 0.05, ***p < 0.001 when comparing samples between $CD11c^{WT}$ and $CD11c^{\Delta raptor}$ mice.

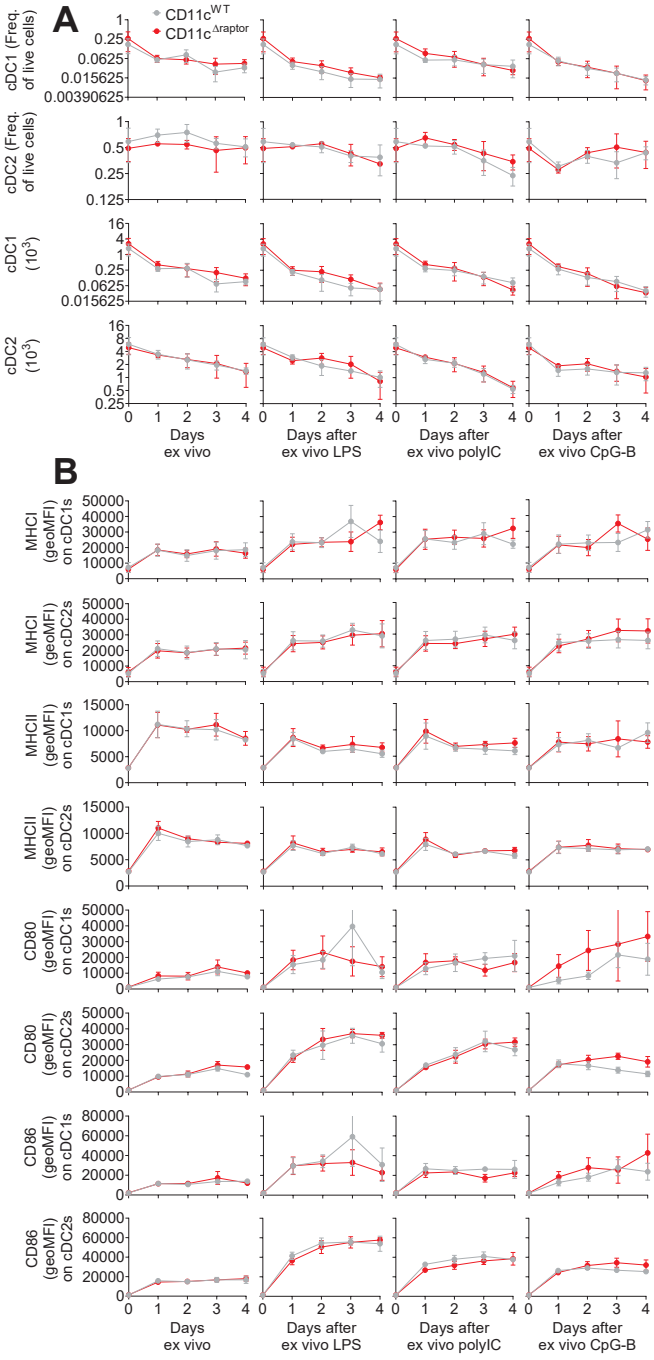
A
CD11c^WT
CD11c^Δraptor
cDC1 (Freq. of live cells)
cDC2 (Freq. of live cells)
cDC1 (10^3)
cDC2 (10^3)
Days ex vivo
Days after ex vivo LPS
Days after ex vivo polyIC
Days after ex vivo CpG-B
B
MHCI (geoMFI) on cDC1s
MHCI (geoMFI) on cDC2s
MHCII (geoMFI) on cDC1s
MHCII (geoMFI) on cDC2s
CD80 (geoMFI) on cDC1s
CD80 (geoMFI) on cDC2s
CD86 (geoMFI) on cDC1s
CD86 (geoMFI) on cDC2s
Days ex vivo
Days after ex vivo LPS
Days after ex vivo polyIC
Days after ex vivo CpG-B

Figure S2.

Splenocytes from naïve $CD11c^{WT}$ and $CD11c^{\Delta raptor}$ mice were stimulated with either 100 ng/mL LPS, 10 µg/mL PolyIC or 5 µg/mL CpG-B and cultured for the indicated time before manual counting and analysis by flow cytometry. (A) Frequencies and numbers of splenic cDCs are enumerated. (B) Splenic cDCs surface protein expression of indicated surface markers. (A-B) Data are from 1 experiment using 4 mice per group (A-B) and shown as mean ± SEM.

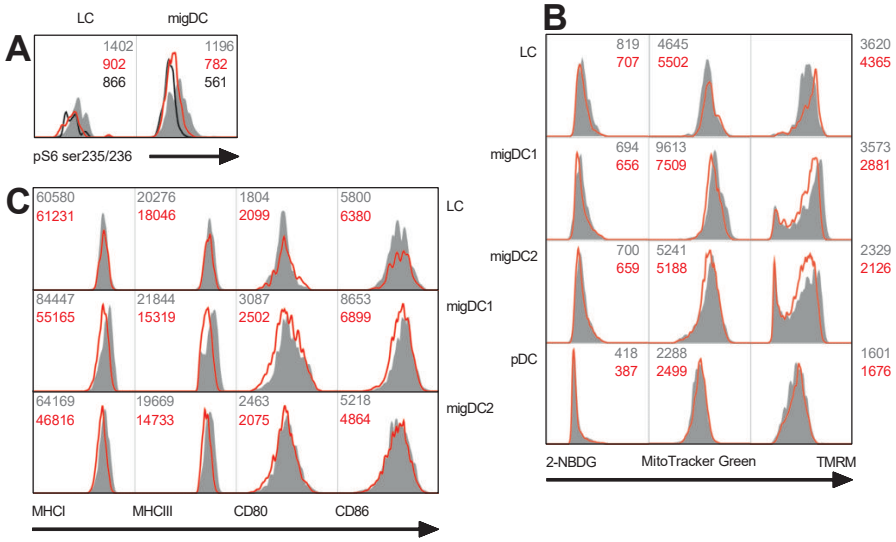

Figure S3.

(A) Representative histograms of S6 phosphorylation in sdLN total migDCs as described in Figure 4B and LCs as described in Figure S6A. (B) Representative histograms of 2-NBDG uptake by sdLN DC subsets and their mitochondrial mass and mitochondrial membrane potential as described in Figure 4D-E, while LCs are described in Figure S6D-E. (C) Representative histograms of indicated surface markers on sdLN migDCs as described in Figure 4F.

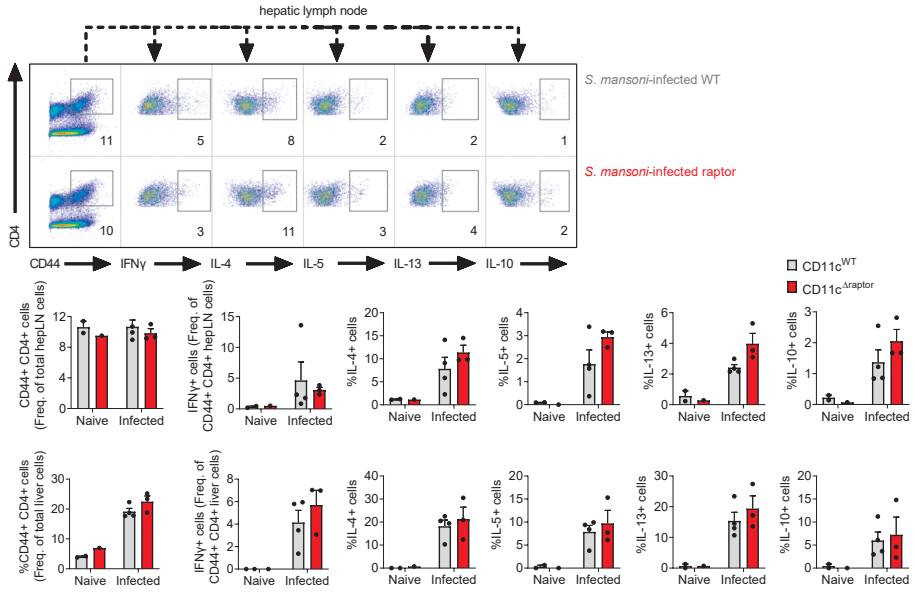

Figure S4.

Mice were infected with *S. mansoni* by percutaneous exposure to cercariae and CD44+CD4+ cell responses were evaluated in livers and draining hepatic lymph nodes eight weeks later. Single cell suspensions were stimulated with PMA/Ionomycin in the presence of Brefeldin A and analysed for production of indicated cytokines. Data are from 1 experiment using 1-4 mice per group and shown as mean ± SEM; $*p < 0.05$ when comparing samples between $CD11c^{WT}$ and $CD11c^{\Delta raptor}$ mice.

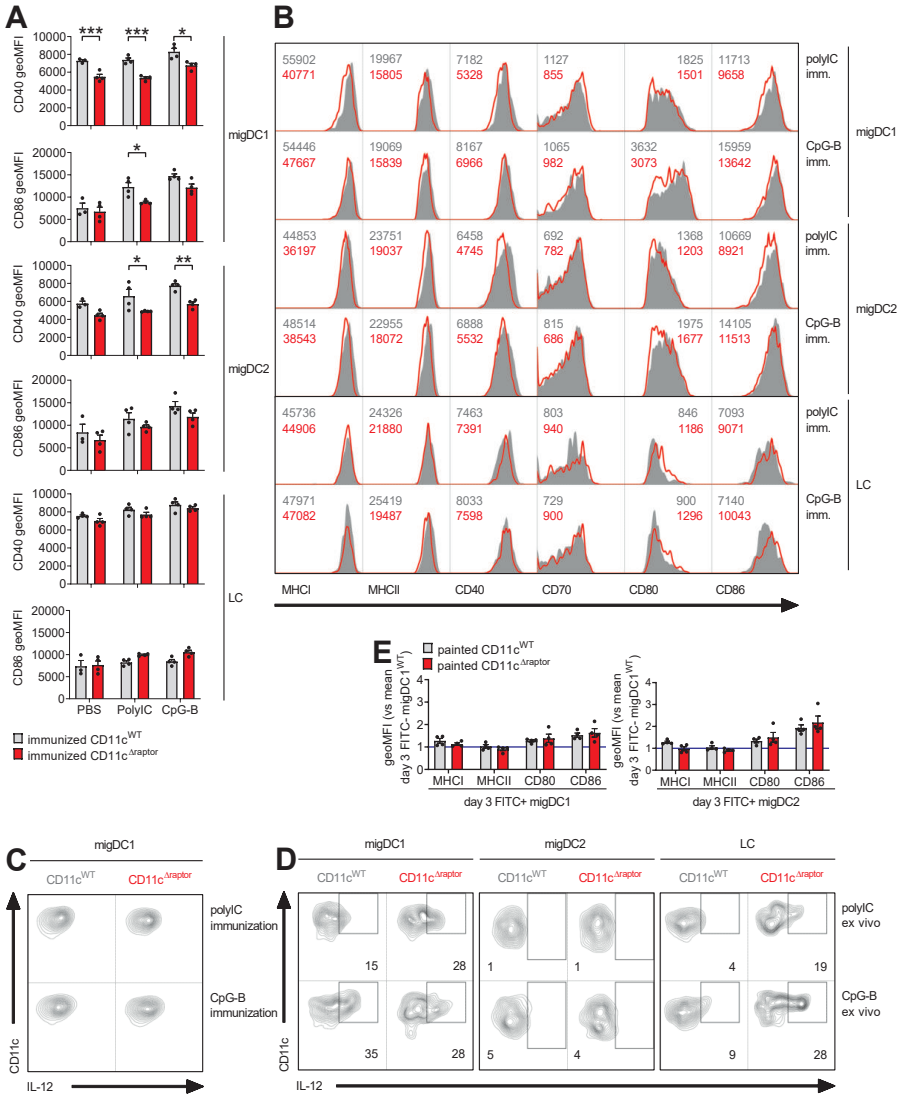
A
CD40 geoMFI
CD86 geoMFI
migDC1
migDC2
LC
PBS
PolyIC
CpG-B
immunized CD11c^WT
immunized CD11c^Δraptor
B
polyIC imm.
CpG-B imm.
migDC1
migDC2
LC
MHCI
MHCII
CD40
CD70
CD80
CD86
E
painted CD11c^WT
painted CD11c^Δraptor
geoMFI (vs mean day 3 FITC- migDC1^WT)
geoMFI (vs mean day 3 FITC- migDC1^WT)
day 3 FITC+ migDC1
day 3 FITC+ migDC2
C
migDC1
CD11c^WT
CD11c^Δraptor
polyIC immunization
CpG-B immunization
CD11c
IL-12
D
migDC1
migDC2
LC
polyIC ex vivo
CpG-B ex vivo

Figure S5.

(A) Same mice as Figure 6A. $CD11c^{WT}$ and $CD11c^{\Delta raptor}$ mice were immunized with either 25 µg of CpG-B or 25 µg of PolyIC by s.c. tailbase injection and migAPC maturation in draining inguinal lymph nodes (ingLNs) was analysed 24 hours later by flow cytometry. (B) Representative histograms of indicated surface markers on sdLN migAPCs as described in Figure 6A,E and S5A. (C) Same mice as Figure 6A. Inguinal LNs were processed and incubated in the presence of Brefeldin A, before analysis of IL-12p40/p70 production by migAPCs, of which only migDC1s is shown, by flow cytometry. (D) Representative histograms of IL-12p40/p70 production by sdLN migAPCs as described in Figure 6B-G. Data is shown as a representative image from one $CD11c^{WT}$ and one $CD11c^{\Delta raptor}$ mouse (same mice as Figure 6A-B, I). (E) Same mice as Figure 6C-D. Mice were painted on their flank with inflammatory FITC paint and FITC+ migDC maturation was analysed on the indicated days by flow cytometry.

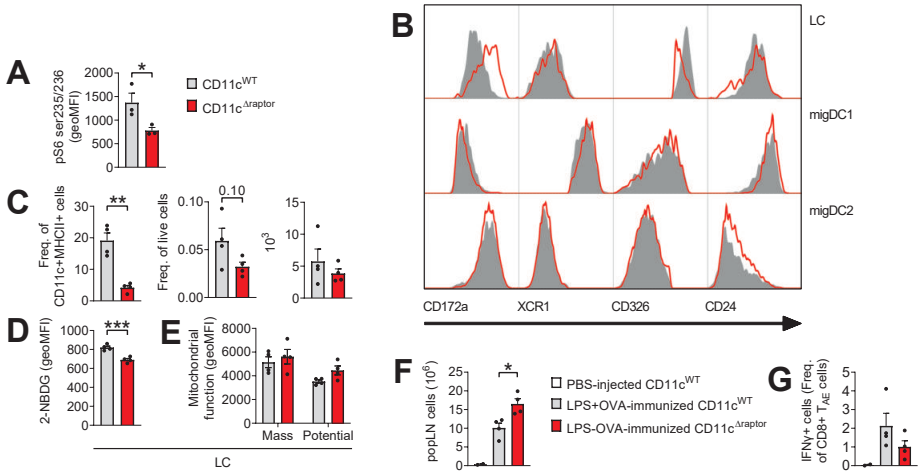

Figure S6.

(A) Flow cytometry-based analysis of S6 phosphorylation on serine 235/236 in LCs from skin draining lymph nodes (sdLNs) out of CD11c^{WT} mice in grey, CD11c$^{\Delta raptor}$ mice in red and a Fluroscence Minus One (FMO control in black). Representative histograms are in Figure S6A. sdLNs were a pool of brachial, axillary and inguinal LNs. (B) Representative histograms of indicated surface markers on sdLN migAPCs as described in Figure 4A with the addition of CD24. (C) Frequencies and numbers of LCs in sdLNs as gated in Figure 4A are enumerated. (D) Flow cytometry-based analysis of glucose uptake by sdLN LCs using the fluorescent glucose analogue 2-NBDG. (E) Flow cytometry-based analysis of mitochondrial mass and mitochondrial membrane potential in sdLN LCs using MitoTracker Green and TMRM, respectively. (F-G) CD11c^{WT} and CD11c$^{\Delta raptor}$ mice were immunized with OVA and 5 µg of LPS by s.c. footpad injection and T cell response in draining popliteal lymph nodes (popLNs) were analysed 7 days later by flow cytometry. (F) Cell counts of popLNs. (G) popLN cells were stimulated with SIINFEKL in the presence of Brefeldin A and analysed for OVA-specific IFNγ production by antigen-experienced CD44+ CD8+ T cells (CD8+ TAE) using flow cytometry. Data are from 1 out of 2 representative experiments (same mice as Figure 4) using 4 mice per group (A, C-E) or from 1 experiment using 2-4 mice per group (F-G) and shown as mean ± SEM; *p < 0.05, **p < 0.01, ***p < 0.001 when comparing samples between CD11c^{WT} and CD11c$^{\Delta raptor}$ mice.

Supplementary tables

Table 1. Antibodies used in study.

Target	Clone	Conjugate	Source	Identifier
CD11b	M1/70	PE-Cy7	Invitrogen/eBioscience	25-0112-82
CD11c	N418	BV421	BioLegend	117330
CD11c	N418	PE-Cy7	Invitrogen/eBioscience	25-0114-82
CD172a	P84	Biotin	BioLegend	144026
CD172a	P84	PE	BioLegend	144011
CD24	M1/69	APC-eF780	BioLegend	101839
CD3	17A2	FITC	Invitrogen/eBioscience	11-0032-82
CD3	17A2	eF450	Invitrogen/eBioscience	48-0032-82
CD3	17A2	BV605	BioLegend	100237
CD326	G8.8	BV605	BioLegend	118227
CD326	G8.8	APC-Fire	BioLegend	118229
CD4	GK1.5	PE-Cy7	Invitrogen/eBioscience	25-0041-81
CD4	GK1.5	PerCP-eF710	Invitrogen/eBioscience	46-0041-82
CD4	GK1.5	BV650	BD Biosciences	563232
CD40	HM40-3	FITC	Invitrogen/eBioscience	11-0402-82
CD44	IM7	eF450	Invitrogen/eBioscience	48-0441-82
CD44	IM7	PE-Cy7	Invitrogen/eBioscience	25-0441-81
CD62L	MEL-14	APC-eF780	Invitrogen/eBioscience	47-0621-82
CD70	FR70	biotin	BioLegend	104603
CD8a	53-6.7	BV711	BioLegend	100747
CD80	16-10A1	PE	Invitrogen/eBioscience	553769
CD86	GL-1	PerCp-Cy5.5	BioLegend	105028
CD8a	53-6.7	APC	Tonbo Biosciences	20-0081-U025
CD8a	53-6.7	APC-Cy7	BioLegend	100714
Goat anti-rabbit	-	AF647	Invitrogen	A27040
HPV tetramer	-	APC	in house	-
LC3A/B	-	Rabbit	Cell Signaling	4108
IFNγ	XMG1.2	PE-Cy7	Invitrogen/eBioscience	25-7311-82
IFNγ	XMG1.2	APC-Cy7	BD Biosciences	561479
IL-10	JES5-16E3	AF488	Invitrogen/eBioscience	53-7101-82

Table 1. Continued

Target	Clone	Conjugate	Source	Identifier
IL-12p40/p70	C15.6	APC	Invitrogen/eBioscience	554480
IL-17A	eBio17B7	APC	Invitrogen/eBioscience	17-7177-81
IL-4	BVD4-1D11	PE	Invitrogen/eBioscience	554389
Kb-SIINFEKL	25-D1-16	PE	BioLegend	141604
MHCI	AF6-88.5	AF647	BioLegend	116511
MHCII	M5/114.15.2	AF700	Invitrogen/eBioscience	56-5321-80
MHCII	M5/114.15.2	APC-eF780	Invitrogen/eBioscience	47-5321-82
OVA tetramer	-	PE	in house	-
pS6 (ser240)	N4-41	PE	Invitrogen/eBioscience	560430
Siglec-H	511	APC	BioLegend	129611
Streptavidin	-	PerCP-Cy5.5	BioLegend	405214
Streptavidin	-	BV605	BioLegend	405229
Streptavidin	-	BV785	BioLegend	405249
XCR1	ZET	BV650	BioLegend	148220
XCR1	ZET	BV421	BioLegend	148216